



## Late Pliocene-Pleistocene incision in the Ebro Basin (North Spain)

Vincent Regard, Arnaud Vacherat, Stéphane Bonnet, Frédéric Mouthereau,  
Jesper Nørgaard, F Knudsen

### ► To cite this version:

Vincent Regard, Arnaud Vacherat, Stéphane Bonnet, Frédéric Mouthereau, Jesper Nørgaard, et al..  
Late Pliocene-Pleistocene incision in the Ebro Basin (North Spain). Bulletin de la Société Géologique  
de France, 2021, 192, pp.30. 10.1051/bsgf/2021020 . hal-03217492

**HAL Id: hal-03217492**

**<https://hal.science/hal-03217492>**

Submitted on 4 May 2021

**HAL** is a multi-disciplinary open access archive for the deposit and dissemination of scientific research documents, whether they are published or not. The documents may come from teaching and research institutions in France or abroad, or from public or private research centers.

L'archive ouverte pluridisciplinaire **HAL**, est destinée au dépôt et à la diffusion de documents scientifiques de niveau recherche, publiés ou non, émanant des établissements d'enseignement et de recherche français ou étrangers, des laboratoires publics ou privés.

# LATE PLIOCENE-PLEISTOCENE INCISION IN THE EBRO BASIN (NORTH SPAIN)

Vincent Regard<sup>1\*</sup>, Arnaud Vacherat<sup>1</sup>, Stéphane Bonnet<sup>1</sup>, Frédéric Mouthereau<sup>1</sup>, Jesper Nørgaard<sup>2</sup>, and Mads F. Knudsen<sup>2</sup>

1. GET, University of Toulouse, UPS (OMP), CNRS, IRD, CNES, 14 av. Edouard Belin, 31400 Toulouse, France

2. Department of Geoscience, Aarhus University, Denmark

\* corresponding author. [Vincent.regard@get.omp.eu](mailto:Vincent.regard@get.omp.eu) / ph. +33 561332645

---

## Abstract

The Ebro Basin constitutes the central part of the southern foreland of the Pyrenees. It was endorheic during the Cenozoic and accumulated sediments. By the end of the Miocene, erosion and river incision reconnected the basin to the Mediterranean Sea, establishing a post-opening drainage network. Those rivers left terraces that we study in this work. We first synthesize previous works on river terraces that are widely dispersed in the basin. We provide new age constraints, up to 3 Ma, obtained thanks to cosmogenic nuclides using both profile and burial methods. We derive a unified fluvial terrace chronology and a homogenized map of the highest terraces over the entire Ebro Basin. The dated terraces labeled A, B, C, D, and E are dated to  $2.8 \pm 0.7$  Ma,  $1.15 \pm 0.15$  Ma,  $850 \pm 70$  ka,  $650 \pm 130$  ka, and  $400 \pm 120$  ka, respectively. The chronology proposed here is similar to other sequences of river terraces dated in the Iberian Peninsula, around the Pyrenees, and elsewhere in Europe. The oldest terraces (A, B, C) are extensive, indicating they form a mobile fluvial network while from D to present, the network was stable and entrenched by 100 to 200 m-deep valleys. The transition from mobile to a fixed fluvial network is likely to have occurred during the Middle Pleistocene Transition (MPT, between 0.7 and 1.3 Ma), when long-period/high-intensity climate fluctuations were established in Europe. We estimate that between 2.8-1.15 Ma and present, the incision rates have tripled.

**Keywords:** Ebro Basin, Middle Pleistocene Transition, Neogene, Fluvial Terraces, Pyrenees, Cosmogenic Nuclides

**Short title:** Mid Pleistocene transition in terrace sequences, Ebro Basin

**Titre en français :** Incision dans le Bassin de l'Ebre (nord de l'Espagne) entre la fin du Pliocène et le Pléistocène

**Résumé en français :** Le bassin de l'Ebre constitue le centre du piémont sud-pyrénéen. Il a été endorhémique et a accumulé une épaisseur importante de sédiments au cours du Cénozoïque. Vers la fin du Miocène, l'érosion et l'incision fluviale ont reconnecté le bassin à la mer Méditerranée, en [établissant](#) un nouveau réseau de drainage. Les rivières constituant ce réseau ont laissé des terrasses que nous étudions dans le cadre de ce travail. Nous faisons d'abord une synthèse des travaux antérieurs sur les terrasses fluviales, qui sont largement dispersées dans le bassin. Ensuite, nous fournissons de nouvelles contraintes d'âge, jusqu'à 3 Ma, obtenues grâce aux nucléides cosmogéniques utilisant à la fois des méthodes de profil d'exposition et d'enfouissement. Enfin, nous en déduisons une chronologie unifiée des terrasses fluviales et une carte homogénéisée des terrasses les plus hautes sur l'ensemble du bassin de l'Ebre. Les terrasses, que nous notons A, B, C, D et E, sont datées respectivement de  $2,8 \pm 0,7$  Ma,  $1,15 \pm 0,15$  Ma,  $850 \pm 70$  ka,  $650 \pm 130$  ka et  $400 \pm 120$  ka. La chronologie proposée ici est similaire à d'autres séquences de terrasses fluviales datées dans la péninsule ibérique, autour des Pyrénées, et ailleurs en Europe. Les terrasses les plus anciennes (A, B, C) sont étendues, ce qui témoigne d'un réseau fluvial mobile alors que depuis la formation des terrasses D jusqu'à aujourd'hui, le réseau était stable et canalisé le long de vallées de 100 à 200 m de profondeur. Le passage d'un réseau fluvial mobile à un réseau fluvial fixe s'est probablement produit pendant la transition du Pléistocène moyen (entre 0,7 et 1,3 Ma), lorsque des fluctuations climatiques de longue période et de forte intensité ont été établies, comme l'ont déjà proposé Gibbard et Lewin (2009) pour les rivières européennes. Nous estimons qu'entre 2,8 et 1,15 Ma et la période actuelle, les taux d'incision ont triplé.

**Mots-clés :** Bassin de l'Ebre, Transition du Pléistocène Moyen, Néogène, Terrasses fluviales, Pyrénées, Nucléides Cosmogéniques

---

## 1 Introduction

Intracontinental endorheic basins (or closed basins) occupy ~20% of the Earth's land surface. They develop mostly in response to the tectonic uplift of surrounding ranges, generally under arid climatic conditions (e.g. Sobel et al., 2003; Garcia-Castellanos et al., 2003) and are infilled by low-erodible sedimentary rocks. They represent key elements of source-to-sink systems as they preserve eroded products from surrounding catchments and large areas, as for the Tibetan Plateau and Tarim basin (Sobel et al., 2003; Han et al., 2019) or the Altiplano (Fornari et al., 2001; Sobel et al., 2003). Characterized by internally-drained depressions they often record the development of a long-lived lake (Altiplano, Titicaca Lake). The opening of an endorheic basin by the capture of internally-drained rivers and lakes has strong implications on the sediment routing and the evolution of the river landscape

(Craddock et al., 2010). Despite the development of analogical and numerical modelling tools, processes by which the river network grows and propagates into a captured endorheic basin remain unclear.

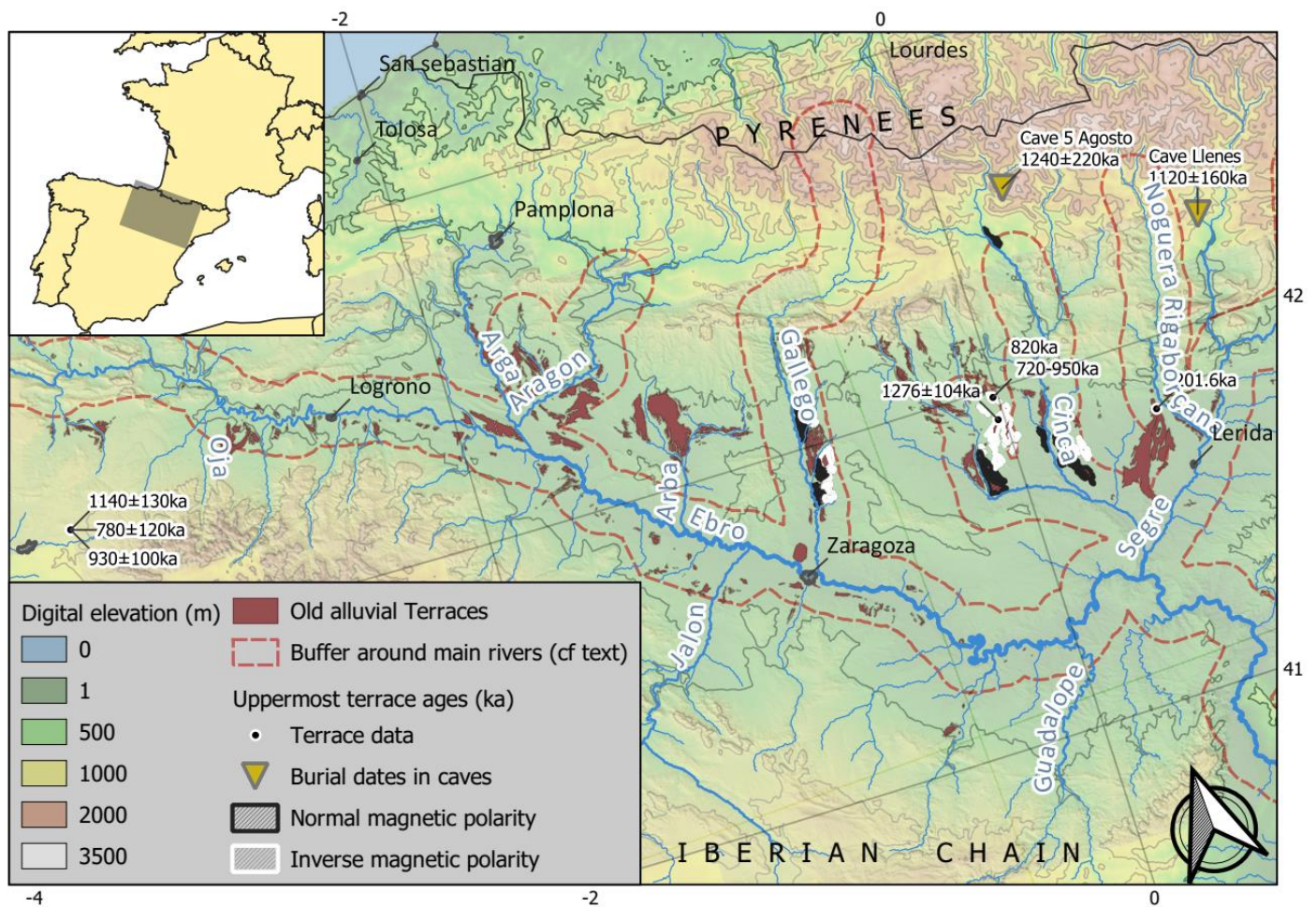


**Figure 1.** Topographic map of Ebro Basin showing the position of topmost terraces together with their ages and paleomagnetic polarity data (Benito et al., 1998; Moreno et al., 2012; Calle et al., 2013; Stange et al., 2013a; Duval et al., 2015; Lewis et al., 2017). Two burial ages in caves from Genti (2015) which are likely related to these topmost terraces are also indicated. The 10-km wide buffer around the rivers serve for the drawing of Figure 6. An enlarged version of this figure can be found on Zenodo (doi:10.5281/zenodo.4721256).

The triangular-shaped Ebro sedimentary Basin in the north-eastern Iberian Peninsula is delimited by the South Pyrenean thrust belt to the north, by the Catalan Coastal Range to the south-east, and by the Iberian Range to the south-west (Figure 1). The basin recorded a long endorheic stage during Oligocene and Miocene times (Puigdefàbregas et al., 1992; Costa et al., 2010). The re-opening of the Ebro Basin toward the Mediterranean Sea led to an incision wave that propagated within the former endorheic basin and the Catalan Coastal Range (e.g. Garcia-Castellanos et al., 2003). The drainage divide delimiting the current Ebro catchment shows numerous evidence of geomorphic disequilibrium suggesting that it is still currently enlarging through drainage network growth, captures, and divide migration (Vacherat et al., 2018; Struth et al., 2019).

In this study, we aim to provide a better resolution of the timing of incision in the Ebro catchment and improving our understanding of the relationships between the morphologic evolution of the Ebro drainage network and the longer-term post-orogenic evolution of the Ebro sedimentary Basin. We first review constraints on Ebro river terrace identifications and ages to propose a consistent terrace chronology scheme throughout the basin. Then, we present new dates for the topmost terraces using in-situ produced cosmogenic nuclides ( $^{10}\text{Be}$  and  $^{26}\text{Al}$ ), hence providing constraints on the most older, i.e. initial, recorded stages of landscape development of the Ebro river network. These new data allow us to track the evolution of the Ebro river network back to the Pliocene.

## 2 Geological setting

### 2.1 Tectonic setting

The Pyrenean orogen resulted from the collision between the Iberian and European continental margins that occurred from the Late Cretaceous to the early Miocene (Choukroune, 1989; Roure et al., 1989; Teixell, 1990, 1996, 1998; Muñoz, 1992; Beaumont et al., 2000; Vergés et al., 2002; Mouthereau et al., 2014). The main period of orogenic growth and exhumation is dated to Eocene-Oligocene (45-30 Ma) (see Yelland, 1990; Morris et al., 1998; Sinclair et al., 2005; Gibson et al., 2007; Jolivet et al., 2007; Rushlow et al., 2013; Labaume et al., 2016). The South Pyrenees thrust sequence shows that deformation propagated from east to west and from north to south since the Late Cretaceous. This orogenic sequence is reflected, north of the Ebro Basin, in the syn-orogenic tectonic-stratigraphic relationships well preserved in the South Pyrenean Zone (SPZ), a classical thin-skin fold and thrust belt made of Mesozoic to Cenozoic sediments detached in the Triassic evaporites (Muñoz, 1992; Vergés et al., 1995, 2002; Mouthereau et al., 2014; Carola et al., 2015; Saura et al., 2016). It was followed by a post-orogenic phase of exhumation reported throughout the Pyrenees at about 10 Ma (Morris et al., 1998; Fitzgerald et al., 1999; Whitchurch et al., 2011; Fillon et al., 2013, 2020; Mouthereau et al., 2014; Bosch et al., 2016; Monod et al., 2016; Huyghe et al., 2020; see also the review by Calvet et al., 2020).

The Iberian chain, south of the Ebro Basin, forms a NW-SE trending doubly vergent intraplate mountain belt. It results from the tectonic inversion of Mesozoic rift basins comprising from east to west the Columbrets, Asturian, Basque-Cantabrian, Maestrat, south Iberian, and Cameros basins (Roca and Guimerà, 1992; Salas and Casas, 1993; Salas et al., 2001; Etheve et al., 2018). Constraints on the recent exhumation pattern of the Iberian chain mainly come from the Cameros basin (Del Rio et al., 2009; Rat et al., 2019). ZFT thermochronological constraints show a minimum age for the inversion initiation of the Cameros basin at ~60 Ma, which is coincident or slightly predates the widespread increase in exhumation rates during the Eocene documented in the Pyrenees. The main exhumation phase is recorded in the Cameros basin at 35–25 Ma coevally with the Pyrenees and the Cantabrian belt (Fitzgerald et al., 1999; Fillon et al., 2016). The increase of exhumation is temporally consistent with



the closure of the connection of the Ebro Basin with the Atlantic Ocean by 36 Ma, leading to the deposition of thick alluvial sediments (Costa et al., 2010). As in the Pyrenees, this exhumation was followed by a Miocene period of planation that resulted in the paleosurfaces still visible on top of the Iberian chain (Calvet et al., 2015). The deposition of late Miocene conglomerates, sealing the main Cameros thrust, was followed by erosion after ~9 Ma (Rat et al., 2019). This result is in agreement with the regional drainage reorganization described throughout the Ebro Basin (Garcia-Castellanos et al., 2003; Fillon et al., 2013, 2020).

The Catalan Coastal Ranges (CCR), located between the Ebro Basin and the Valencia Trough, formed by the tectonic inversion of Mesozoic rift basins during the Paleogene, contemporaneously with the Pyrenean orogeny (Salas et al., 2001; Gaspar-Escribano et al., 2004). From Late Oligocene onward, extension in the Valencia Trough associated with opening of the Gulf of Lion led to the development of ENE-WSW to NE-SW-striking horst and graben, triggering uplift (Lewis et al., 2000; Garcia-Castellanos et al., 2003).

During the Late Eocene, uplift in the Western Pyrenees (Muñoz et al., 1986; Puigdefàbregas et al., 1992) closed the Ebro Basin. This resulted in a sudden increase of sedimentation rates and continentalization of the endorheic basin (Costa et al., 2010). The deposition of a large amount of coarse alluvial deposits (Coney et al., 1996; Babault et al., 2005b) from Bartonian to Late Oligocene (Beamud et al., 2003, 2011) filled the paleovalleys that developed at the front of the South-Pyrenees (Vincent, 2001). Such conglomeratic bodies are also observed against the Catalan Coastal Range and the Iberian Range. The center of the Ebro basin became a long-lived lake filled with lacustrine and sandy deposits during the Oligocene and the Miocene (Pérez-Rivarés et al., 2002, 2004; Garcia-Castellanos et al., 2003; Garcia-Castellanos, 2006; Larrasoña et al., 2006; Vázquez-Urbez et al., 2013).

In the Pyrenees, in addition to the low temperature thermochronology data already mentioned, post-10 Ma uplift is suggested by geological data (Calvet et al., 2020) including recent paleoelevation estimates (e.g. Huyghe et al., 2020). This uplift is consistent with the reconstruction of the evolution of river profiles suggesting a post-30 Ma incision of the whole of Iberia (Conway-Jones et al., 2019). In the absence of significant crustal shortening, the drivers of this post-10 Ma uplift are heavily debated. They include changes related to increasing temperature in the asthenospheric mantle, regional scale mantle flow, lithospheric folding, or magmatic addition in the lithospheric mantle (Cloetingh et al., 2002; Boschi et al., 2010; Faccenna et al., 2014; Conway-Jones et al., 2019; Huyghe et al., 2020).

## 2.2 Timing of Ebro Basin opening to the Mediterranean Sea

The timing and factors controlling the opening of the Ebro basin toward the Mediterranean Sea have long been debated, mainly due to the limited chronological constraints. Extension in the Catalan Coastal Range (CCR) triggered rift flank uplift, which, together with dry climatic conditions, favored the endorheic basin stage (Garcia-Castellanos et al., 2003). This extension finally resulted in the Valencia

Trough opening during Miocene (Fontboté et al., 1990; Roca et al., 1990, 1999; Sàbat et al., 1995; López-Blanco, 2002). Coney et al. (1996) proposed that the Valencia Trough opening was responsible for the capture of the Ebro paleo-lake. Seismic and sedimentary analysis of the Ebro delta in the Valencia Trough have shown that the first record of siliciclastic sediments coming from the Iberian margin is Serravalian-Tortonian in age (Castellon Group, Evans and Arche, 2002). Garcia-Castellanos et al. (2003) then proposed that the age and amount of sediments preserved in the Valencia Trough are consistent with an onset of basin opening between 13 and 8.5 Ma, further facilitated by wetter climatic conditions that increased base level in the paleo-lake. The timing of basin opening has been refined to 12-7.5 Ma by combining the flexural isostatic compensation of the eroded volume with available constraints on sediment age (Garcia-Castellanos and Larrasoña, 2015). This timing of basin incision is coherent with low-temperature thermochronological studies reporting AHe cooling ages from the SPZ (Fillon et al., 2013) and AHe ages from the western Axial Zone in the Pyrenees (Bosch et al., 2016; Fillon et al., 2020) documenting post-orogenic exhumation between 9 and 11 Ma. In its lower reaches, the Ebro seems to have crossed the CCR before the Messinian Salinity Crisis (MSC), as evidenced by clasts sourced from the Pyrenees (Arasa-Tuliesa and Cabrera, 2018). The MSC did not lead to the entrenchment of the Ebro at the bottom of a deep canyon, unlike what has been observed for the Nile (Chumakov, 1967) and the Rhone (Loget et al., 2005; Mocochain et al., 2009). This issue was resolved by detailed offshore seismic constraints that document canyons buried offshore in the Ebro delta filled by pre-Messinian sediments (Urgeles et al., 2011). Based on the above arguments, we consider the Ebro Basin opening toward the Mediterranean Sea occurred between 7.5 and 13 Ma (see also Calvet et al., 2020 for a synthesis).

Beyond the issues about the age of incision of the Ebro Basin and whether its capture is related to sediment overfilling or headward retreat incision (Garcia-Castellanos et al., 2003), little is known about the evolution of a river network after the onset of the capture of Ebro basin.

## 2.3 Ebro Basin paleoclimates

At the beginning of our study period, during the Miocene, the climate of the Ebro basin was subtropical and dry (López Martínez et al., 1987; Barrón et al., 2010), favoring the development of endorheic lakes (Garcia-Castellanos, 2006). During the Middle-Late Miocene and Early Pliocene, northern Iberia recorded alternations of cold-wet and hot-dry periods (i.e., Bessais and Cravatte, 1988; Barrón et al., 2010). Afterwards, the Panama Isthmus closure at ~3 Ma induced the establishment of the present-day oceanic circulation and global climate (cf. Maier-Reimer et al., 1990; Haug and Tiedemann, 1998; Molnar, 2008). This led, during the Quaternary, to more humid and colder climate conditions characterized by dry glacial periods and humid interglacials, especially for the Mediterranean area (Suc and Popescu, 2005; Jiménez-Moreno et al., 2013). Finally, during the Lower-Middle Pleistocene

Transition (MPT, ~1.3-0.7 Ma), the dominant orbital periodicity changed from 41 ka to 100 ka (Tziperman and Gildor, 2003; Lisiecki and Raymo, 2005; Siddall et al., 2010).

## 2.4 Review of Ebro Basin fluvial terraces, with emphasis on the topmost terraces

In the Ebro Basin, the flights of fluvial terraces along the main rivers and tributaries are widespread and can be organized to first-order into two groups (e.g. Lucha et al., 2012). The most elevated terrace levels (Figure 1), at >100-150 m above the current river level, consist of widespread and high-elevation pediment surfaces covered by up to ~20 m of rounded pebbles of varying lithology. These upper levels are often located at the summit of hillcrests and seem locally disconnected from the present drainage network (e.g. Bomer, 1979). On the opposite, below ~120 m, most of the terrace levels have a limited extent within modern valleys and along river courses. This morphological break highlights a transition between wandering fluvial systems with efficient lateral planation and beveling capabilities (e.g. Cook et al., 2014; Bufo et al., 2016, 2017) to entrenched and more stable river courses (e.g. Bomer, 1979). The term “mobile” refers to lateral river mobility, enhancing lateral erosion, whose greatest effect is valley widening up to the beveling of large platforms. For example, the Barbastro-Balaguer anticline has been completely flattened during the setup of these high levels (Lucha et al., 2012) before being subsequently entrenched by the Cinca, Noguera-Ribargorzana, and Segre rivers. The contrasting behaviour of the rivers after this transition is well illustrated by the terraces sequences of the Cinca (Lewis et al., 2017) or Alcanadre rivers (Calle et al., 2013). It may correspond to a transition from a depositional stage under sub-arid conditions, toward a more erosive stage characterized by a more focused incision. This could correspond to the climatic change recorded during the Lower-Middle Pleistocene transition (e.g. Stange et al., 2016). The formation of terraces younger than the Middle Pleistocene transition appears to be related to global climatic cycles (e.g. Macklin et al., 2002; Santisteban and Schulte, 2007; Arboleya et al., 2008), though other parameters such as uplift may be also important in defining the number of terraces and their altitudinal distribution (Santisteban and Schulte, 2007).

Due to the marked interest in the relationship between the incision and glacial cycles, most previous studies in the Ebro and Duero basins have focused on the lowest terrace system, close to the actual course of the rivers (e.g. Lewis et al., 2009; Calle et al., 2013; Stange et al., 2013a, 2013b). In addition, the lower terraces are much easier to date with classical methods like OSL, TL, ESR,  $^{10}\text{Be}$  cosmnuclide, and even  $^{14}\text{C}$ , usually much more efficient for ages under 300 ka (e.g., Fuller et al., 1998; Lewis et al., 2009, 2017; Calle et al., 2013; Stange et al., 2013a; Duval et al., 2015, 2017; Sancho et al., 2016, 2018; Delmas et al., 2018; Soria Jáuregui et al., 2019).

The highest preserved terraces levels in the Ebro and Duero basins, supposed to be the oldest evidence of fluvial incision, have often been considered as regionally coeval based on their elevation only (Bomer,



1979; Julián Andrés, 1996; Santisteban and Schulte, 2007; Lucha et al., 2012). This relative approach is important because dates alone sometimes do not allow deciphering the various terraces. Moreover, these dates are difficult to obtain. They are mainly derived from ESR, magnetostratigraphy, and more recently cosmogenic pairs of nuclides (Figure 1). In the following paragraphs, we review the labels and dates of these highest levels and the chronological transition toward the lower levels, i.e. when the river began to entrench. We adopt a roughly East-West progression, first for the Pyrenean (northern) reaches and then for the southern reaches.

Along the Segre river flowing from the Pyrenees, 8 levels of terraces have been documented (Stange et al., 2013b), as well as in its major tributary, the Noguera Ribagorçana. The three top-most terrace levels are covering the interfluvium to the west in between the Noguera Ribagorçana and the Cinca Rivers (the “highest” levels described before; Bomer, 1979; Stange et al., 2013a) but have not been documented along the Segre river. These three top-most terraces are characterized by important cementation (Bomer, 1979; Delmas, 2019). They lie 110-160 m above the present-day Noguera Ribagorçana river course (Bomer, 1979; Lucha et al., 2012; Stange et al., 2013a). The uppermost level has been dated to be ~200 ka BP by inversion of  $^{10}\text{Be}$  depth profiles by Stange et al. (2013a) (Figure 1), but this date is questioned regarding the inversion technique adopted (Delmas, 2019) and the correlation with the Ebro high fluvial terraces (see below, Bomer, 1979; Lucha et al., 2012). In the upper Noguera Pallaresa, a tributary of the Segre, cave deposits were recently dated using the cosmogenic burial method to ~1.1 Ma ( $^{26}\text{Al}$ ,  $^{10}\text{Be}$  pair in Llenes cave, ~100 m above the current river course, Figure 1)(Genti, 2015).

Along the Cinca river, 10-11 terrace levels are documented (Bomer, 1979; Peña-Monné and Sancho, 1988; Santisteban and Schulte, 2007; Lewis et al., 2009, 2017). The two topmost levels are equivalent to the three topmost levels mentioned to the west of the Noguera Ribagorçana valley. They are labelled Qt1 and Qt2 by Santisteban and Schulte (2007) and are ~180 m and ~130 m, respectively, above the present-day river course. The terrace level immediately below (Qt3 in Santisteban and Schulte, 2007), shows a normal magnetic polarity whereas Qt1 and Qt2 polarities are reverse. In addition, based on the degree of soil weathering, Lewis et al (2017) proposed an age of  $401 \pm 117$  ka for Qt3. Qt5 is dated to  $178 \pm 21$  ka (OSL, Lewis et al., 2009) and Lewis et al. (2017) estimate likely ages of 999-1070 ka and 780-999 ka for Qt1 and Qt2, respectively, on the basis of paleomagnetic data. ESR analyses were also performed on these terraces, yielding ages of ~1.3 and ~0.8 Ma for Qt1 and Qt2, respectively (Duval et al., 2015; Sancho et al., 2016). Remnants of Qt1 and Qt2 are located on the interfluvium between the Cinca and the Alcanadre rivers (Figure 1).

The Alcanadre river is the next main river to the west and is a tributary of the Cinca river. 9 terrace levels have been mapped along the Alcanadre river. The two topmost levels, Qt1 and Qt2 were presented in the preceding paragraph. They lie at 160-200 m and 100-190 m, respectively, above the present-day

Alcanadre river, and are characterized by inverse magnetic polarity (Calle et al., 2013; also dated with ESR as discussed in the following Duval et al., 2017) (Figure 1).

The next river to the west is the Gállego river. 10 to 12 terraces are described along its course (Benito et al., 2000, 2010; Santisteban and Schulte, 2007 and references; Lewis et al., 2009). The 5-6 uppermost levels are older than the Brunhes-Matuyama transition. The Brunhes-Matuyama transition is at ~150 m above the current Gállego river (Santisteban and Schulte, 2007). To the south of the city of Zaragoza, the Rio Huerva displays a similar, well-developed terrace sequence up to 150 m above the river course, but not dated (Guerrero et al., 2008). The highest terraces described along the Ebro river course are those found close to Zaragoza (Benito et al., 2000) and 30 km downstream (T1 and T2 ~200 m above the current Ebro course, Guerrero et al., 2013) (Figure 1). Locally, the terrace sequence is disturbed by karstic processes; this is particularly true in the Zaragoza area (Mensua and Ibañez, 1977; Benito et al., 1998, 2000; Guerrero et al., 2008, 2013). These remarks probably explain that the important Gállego set of terraces do not appear in large-scale correlation (e.g., Santisteban and Schulte, 2007).

The last important tributary sourced from the Pyrenees is the Aragón river. It has been mostly studied in its upper reaches in the mountain, for the glacially-derived terraces (García-Ruiz et al., 2013). Along its course within the Ebro Basin, Bomer (1979) indicates 5 fluvial terraces. The topmost one lies 120-140 m above the present-day river and builds a large plateau testifying for a mobile river when it formed. This terrace is likely equivalent to the large set of terraces found at the top of the Ribagorzana and Cinca valleys (Bomer, 1979). In its lower part, it is highly deformed by diapiric movements (Casas et al., 1994). To the north of the Aragón river, along its Cidacos tributary, an extensive terrace sequence is preserved (Figure 1). The difference in elevation of the Cidacos terraces appears to increase towards the Ebro Basin.

In the upper reaches of the Ebro river, high terrace levels surrounded by glacis are observed (Soria Jáuregui et al., 2019). In the Duero basin, close to the drainage divide with the Ebro Basin (Vacherat et al., 2018), the highest Arlanzon river terraces T3, T4, and T5, were dated, using ESR, between 1.1 Ma, and ~0.6 Ma (Moreno et al., 2012)(Figure 1).

To the south, numerous rivers with documented terraces are draining toward the Ebro, like the Najerilla river, which has a well-preserved terrace record composed of 10 levels, but with sparse chronological information (Julián Andrés, 1996) (Figure 1). The only one southern tributary with chronological data is the Guadalupe river whose terrace record comprises 13 levels with some IRSL chronological up to 250 ka BP (Fuller et al., 1996, 1998). Along the Guadalupe river, the uppermost terraces, lying ~56 and 81 m above the current river stream, could be equivalent to the topmost terraces along the Cinca and Gállego valleys (Santisteban and Schulte, 2007).

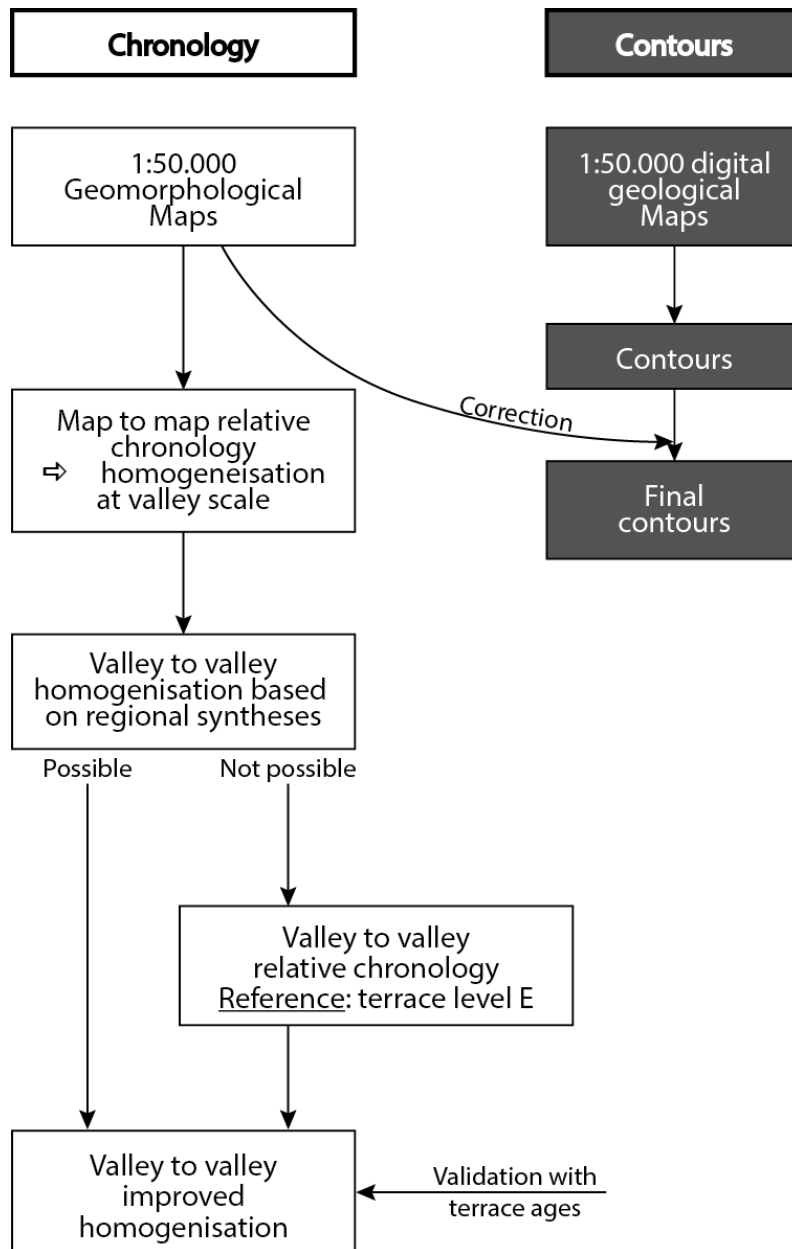


**Figure 2. Schematic workflow for terrace mapping (contours) and chronology.**

### 3 Methods

#### 3.1 Towards a unified model of Ebro terrace succession

There has been a little attempt, so far, to provide a unified model of terrace succession over the Ebro drainage basin. Tentative correlations have been proposed however in some parts of the basin, mainly along the Segre and its tributaries: Alcanadre, Cinca, Noguera Rigaborçana (Bomer, 1979; Alberto et al., 1983; Stange et al., 2013b). Rare correlations between terraces along distant valleys were proposed, like the correlation between the Gállego and Alcanadre river terrace sequences (Mensua and Ibañez, 1977; Lewis et al., 2017) or the one between main river terraces on both sides of the Pyrenees (Delmas et al., 2018; improved from Cordier et al., 2017). No attempt was made to correlate with fluvial terraces

further west, probably because of the distance and because the area of Zaragoza and the Gállego valley is disturbed by local deformations produced by the mobilization and dissolution of evaporite (Benito et al., 1998, 2000; Guerrero et al., 2008, 2013).

We have correlated and unified the terrace labels over the entire basin at a scale of 1:50,000 (workflow on Figure 2). We have first considered individual geographical areas (usually a valley) before to evaluate correlations between the successive locations. At the valley scale, we used georeferenced 1:50,000 geomorphological maps (Mapa Geomorfológico de España a escala 1:50.000 published by IGME; UTM 30 or 31 reference system; [info.igme.es/cartografiadigital/tematica/Geomorfologico50.aspx?language=es](http://info.igme.es/cartografiadigital/tematica/Geomorfologico50.aspx?language=es)). These maps contain a detailed mapping of the terraces and a nomenclature in alphabetical order starting with 'a' for the oldest terrace. The terrace layouts (polygons) were taken from the digital geological map (MAGNA 50 - Mapa Geológico de España a escala 1:50.000 (2ª Serie) with shapefiles, IGME; <http://info.igme.es/cartografiadigital/geologica/Magna50.aspx>) when the contour on the geomorphological map corresponded to the boundaries on the digital geological map (Figure 2). When the difference between the two was judged to be too large, we manually retraced the contour of the terrace as drawn on the geomorphological map. In the rare case of disagreement from one map to another for a single valley, we chose to join or instead distinguish between entities. These geomorphological maps cover only ~20% of the basin, but most of the main valleys east of Zaragoza. In the areas not covered, we relied on the geological map and manual contouring of flat areas from the shaded DEM (MDT25 dataset from IGN) and derived slope map (Figure 2).

The mapping of terraces has been improved by comparison with published works on the terraces of the studied valleys (e.g. Benito et al., 2000; Stange et al., 2013b; Lewis et al., 2017), as well as broader syntheses from which we georeferenced the main synthesis maps (e.g. Alberto et al., 1983; Benito et al., 2000; Calle et al., 2013) (Figure 2).

This work of detailed mapping focused only on the highest terraces. We did not include any terraces in the immediate vicinity of the active stream, either geographically or in terms of elevation (<50 m difference in elevation). Based on geological and geomorphological maps and published works (e.g. Lewis et al., 2017), we have verified that *a priori* all the terraces older than 300-400 ka were mapped. This work resulted in more than 500 polygons, with ~250 of them being associated with a terrace level identified in the published geomorphological map or identified in a publication.

The second part of the work was to correlate the sequences of terraces. For the multiple tributaries of the Segre to the east, this work has been facilitated by the number of previously published works and existing geomorphological maps, although without any real homogenization for terrace labels (see Stange et al., 2013a). Similarly, the sequence of the Gállego is well defined (Benito et al., 1998, 2000). We correlate these two areas based on the mapping by Alberto et al. (1983) of the high terraces and the

one by Mensua and Ibañez (1977) of the terraces and glacis in a large area around Zaragoza. For the Aragón and Ebro valleys, the sequences of terraces are far from the Segre/Gállego area. Despite this difficulty, we established a correlation which is first based on the lower sequence, in particular the level E, a large ubiquitous level that can be found in every valley of the Ebro Basin. This correlation is then refined on the basis of differences in altitude between the terraces (e.g. Julián Andrés and Chueca Cía, 1998), degrees of preservation, and an attempt of correlation by Bomer (1979), who correlated the topmost surfaces of the Segre and the Aragón valleys based on their geomorphological position and the presence of highly cemented conglomerates.

At the end of this work, certain ambiguities remained. Ultimately, to resolve these ambiguities, we have used the ages and magnetic polarities published in the literature as well as the new age constraints presented below (Figure 2). The latter adjustments are proved to be minor, indicating our homogenisation procedure is quite robust. A few remaining mismatches reveal a potential error limited to a difference of one level. Differences in terrace level recognition also occur between our map and one of the published ones, or between two different publications (for example between the maps from Mensua and Ibañez, 1977 and from Alberto et al., 1983). Following our terrace mapping workflow, we labeled each terrace level using capital letters, similar to the convention used on geomorphological maps and deliberately different from the labels used in publications, which are different for each river studied. The shapefile is available at [doi:10.5281/zenodo.4721256](https://doi.org/10.5281/zenodo.4721256).

### 3.2 Cosmogenic nuclide dating methods used (depth profiles and P-PINI)

In-situ cosmogenic nuclides are produced within the Earth's surface material through nuclear reactions (mostly spallation but also muonic capture) promoted by cosmic rays. Spallation processes occur within a couple of meters below the Earth's surface (e.g., Lal, 1991; Gosse and Phillips 2001). The concentration of *in situ*-produced (i.e., produced within the crystal lattice) reflects the time the mineral spent in the production zone (c.a. from surface to few upper meters below surface). They have been extensively used for dating alluvial surfaces, assuming that both the initial mineral concentration at deposition time (thereafter called inheritance) and the denudation rate of the alluvial terrace are negligible (e.g., Bierman et al., 1995; Brown et al., 1998; Regard et al., 2005). For old terraces (>300 ka), surface reworking may be quite significant. To overcome this problem and avoid inheritance effects, it is advisable to analyze the depth profiles of cosmogenic nuclide concentration (e.g., Anderson et al., 1996; Repka et al., 1997; Ritz et al., 2003; Hidy et al., 2010), although this cannot allow to date terraces much older than 500 ka. For longer timescales, cosmogenic nuclides can be used by pairs. The analysis is very different in this case: the two cosmogenic isotopes are produced in a similar fashion in the same mineral during his life nearby the Earth's surface, allowing the knowledge of their initial concentration ratio. Then, the mineral is buried far from the surface, where cosmogenic nuclide production is



negligible. Thus, the concentration ratio evolves following the various disintegration rates of the two cosmogenic nuclides. This method is called burial method (Balco and Shuster, 2009). It may be modified to take into account the production after the mineral has been buried, which has been popularized under the name of isochron method (Balco and Rovey, 2008). This method allows dating alluvial terraces up to a couple of million years (e.g., Balco and Shuster, 2009; Jungers and Heimsath, 2016).

In this paper, we report new chronological constraints obtained with various cosmogenic nuclide techniques: exposure depth profiles, simple burial and P-PINI, which is an adaptation of the isochron burial method.

### 3.2.1 Basic systematics

The basics of cosmogenic nuclide systematics can be found in Gosse and Phillips (2001) and Dunai, (2010). We sum up in the following the most important information. Cosmogenic nuclides are produced at Earth's surface by secondary cosmic rays (neutrons muons). Cosmic rays are quickly absorbed at depth, so that the production rate exponentially decreases against the mass of overlying material:  $P(z) = P_0 e^{\rho z / \Lambda_i}$ , where  $P_0$  is the surface production rate ( $\text{atom.g}^{-1}.\text{yr}^{-1}$ ),  $\rho$  the density ( $\text{g.cm}^{-3}$ ), and  $\Lambda$  ( $\text{g.cm}^{-2}$ ) corresponds to the attenuation length of cosmic-ray particles. Production accounts for three types of secondary cosmic rays: neutrons, slow muons and fast muons (thereafter corresponding to  $i=1, 2$  and  $3$ , respectively). At an alluvial surface, the concentration  $C$  in cosmogenic nuclide depends on the age of the alluvial surface ( $t$ ), its erosion rate ( $\epsilon$ ) and the initial cosmogenic nuclide content, often called inheritance ( $H$ ), and the decay constant ( $\lambda$ ):

$$C(t) = H e^{-\lambda t} + \sum_i \frac{P_0 e^{\rho \epsilon / \Lambda_i}}{\lambda + \rho \epsilon / \Lambda_i} (1 - e^{-(\lambda + \rho \epsilon / \Lambda_i)t})$$

If  $t$  and  $\epsilon$  are unique for a single terrace,  $H$  varies for each sample. To determine the most probable ( $t, \epsilon$ ) pair, depth profiles are often used. Numerical processing of concentration vs. depth data is not straightforward and numerical procedures have been proposed, in particular, the one we used, developed by Hidy et al. (2010). They explore ( $t, \epsilon$ ) pairs and select the most probable ones by minimizing the difference between the observed and modelled concentrations.

Input parameters in the program provided by Hidy et al. (2010) are a density of 2 to 2.4  $\text{g.cm}^{-3}$ , a neutron attenuation length of  $160 \pm 10 \text{ g.cm}^{-2}$  and a minimum number of profiles tested of 100,000. Other site-dependent input parameters were fixed after a few iterations to encompass all the range of the likely values. They are the explored age range, the maximum erosion rate, an erosion threshold. We also set the maximum inheritance to a value close to the minimum measured concentration.

Different cosmogenic nuclides can be used. For quartz-rich lithologies, the most convenient one is  $^{10}\text{Be}$ . Interestingly,  $^{26}\text{Al}$  can be also used.  $^{10}\text{Be}$  and  $^{26}\text{Al}$  are produced proportionally; the radioactive decay of  $^{26}\text{Al}$  being is approximately twice as fast as the  $^{10}\text{Be}$  (half-lives of 0.705 and 1.387 Ma, respectively).

Consequently, the concentrations of surface samples in  $^{10}\text{Be}$  and  $^{26}\text{Al}$  are linked (their ratio  $R$  is  $\sim 6.6$  if their source area denudation rate is not too slow). If buried, it is possible to record the burial time by recording the evolution of the ratio in the two nuclides, following their disintegration. The burial must be at high depth, far below the surface, where there is no more cosmogenic nuclide produced. This holds true for depth  $> 10$  m. On the contrary, it is possible that production during burial is not negligible in alluvial sequences, thus the burial duration is a minimum estimate. It is possible to correct for this post-burial production by comparing the concentration in cosmogenic nuclide of various rocks sampled at a similar depth, following a method called isochron (e.g., Balco and Rovey, 2008; Jungers and Heimsath, 2016). P-PINI (Particle Pathway Inversion of Nuclide Inventories) is an adapted isochron method that has been recently setup to account for complex pre-burial histories (Knudsen et al., 2020). The P-PINI method applies a Monte Carlo source-to-sink model approach, in which a large range of possible exposure and erosion histories are simulated for both the source and sink areas. For the source area, this involves highly complex exposure histories and abrupt erosion events associated with the presence of ice covers. The source model thus includes three episodes of ice cover with durations ranging from 2-100 ka for the two former ones and 2-10 ka for the latter one. These ice-covered periods are characterized by a complete halt in the production of cosmogenic nuclides, and a stochastic erosion event with an erosion depth randomly selected from the range 1 cm - 10 m. Periods with no ice cover are characterized by the production of cosmogenic nuclides with a range of production rates that corresponds to the elevation range of the estimated source area. The ice-free periods are accompanied by uniform and continuous erosion with rates randomly selected from the range 1-1000 m/Ma. Each simulation of the exposure and erosion history in the source area produces a ( $^{26}\text{Al}$ ,  $^{10}\text{Be}$ ) nuclide pair that is used as input for the sink model. This model simulates a large range of possible burial ages, assuming that the sediments were not covered by ice after deposition and that they experienced continuous erosion with rates in the range 1-500 m/Ma throughout the burial period. The production rate in the sink model corresponds to the location and elevation of the study site after correction for the sampling depth. Altogether, the combined P-PINI model approach includes  $1 \times 10^7$  simulations for each study site, and a method known as rejection sampling is used to accept simulations that yield  $^{10}\text{Be}$  and  $^{26}\text{Al}$  concentrations that agree with measured concentrations. P-PINI includes the production of  $^{10}\text{Be}$  and  $^{26}\text{Al}$  associated with spallation, negative muon capture, and fast muons. A full in-depth description of the P-PINI model approach can be found in Knudsen et al. (2020).

### 3.2.2 Sampling sites

#### 3.2.2.1 Segre terraces

The highest Segre river terrace is characterized by a large,  $\sim 30$  km long pedimentation surface pediment striking NNW – SSE made of three distinct sub-levels, lying on the interfluvium between the Noguera Ribagorçana and Cinca rivers (Bomer, 1979; Lucha et al., 2012; Stange et al., 2013a, 2013b). This set of surfaces is limited to the north, by the South Pyrenean Frontal Thrust (SPFT), close to the upstream

valley of the Noguera Ribagorzana river. The highest Segre river terrace levels the Barbastro-Balaguer anticline, which outlines the SPFT (Lucha et al., 2012). The organization of terrace remnants suggests an eastward shift of the Noguera Ribagorzana during deposition.



**Figure 3. TSEG1 (0.551336°E, 41.83316°N, 389 m, top left), TSEG2 (0.573069°E, 41.70244°N, 357 m, top right), and TALC1 (-0.034394°E, 41.908655°N, 486 m) outcrops.**

From these three alluvial surfaces, the level Qt0a (B in our terminology, see thereafter), where TSEG2 has been collected (0.573069°E, 41.70244°N, 357 m; Figure 3), is the highest, ~160 m above the present-day Noguera Ribagorzana river. It consists in ~10 m thick of gravels deposited on top of Oligocene strata, with intercalation of sandy channels, topped by a very thin soil layer (< 10 cm).



Although the top surface is flat, it is slightly dipping towards the valley indicating lateral erosion on the edges. We collected 6 samples along a depth profile from 15 to 380 cm from the surface (TSEG2, Figure 3). We choose a sampling site with a relatively flat top to minimize post-deposition erosion, on an ancient quarry site west of the locality of Rossello.

We also sampled (TSEG1) the lowest of these uppermost levels, Terrace Qt1 (D in our terminology). This terrace is situated at ~115 m above the present-day active channel of the Noguera Ribagorzana river. It consists of polygenic imbricated conglomerates overlying Oligocene strata. The top of this section (from 0 to ~30 cm) is cemented by a calcrete as mentioned by Bomer (1979). TSEG1 (0.551336°E, 41.83316°N, 389 m) consists in 7 samples along a depth profile from 15 to 300 cm from the surface (Figure 3). The sampling site, south to the Alfarras locality, is a small ancient quarry with no evidence of important surface erosion.

#### 3.2.2.2 Alcanadre terrace

Sample TALC1 (-0.034394°E, 41.908655°N, 486 m) comes from an upper terrace level that forms the divide between the Alcanadre and Cinca rivers (Terrace Qt1 of Calle et al., 2013; Duval et al., 2015). This large terrace (~15 km long; B terrace level, see the following) is gently sloping southward (0.5 %). Its elevation above the modern Alcanadre river decreases from 200 m to the North to 160 m to the south. At the sampling place, to the SW of Peralta de Alcofea, the top of the terrace is at 176 m above the current river. Samples come from a thick (> 10 m) succession of conglomerates with well-rounded gravels and pebbles in a sandy matrix and occasional large cross-beddings and sand lenses (Figure 3). The upper part shows the development of thick soil (~3 m) with massive calcrete. Sample TALC1 consists of quartz pebbles and sand taken at depth of 8.50 m below the top of the terrace. Paleomagnetic data of Calle et al. (2013) indicate normal magnetic polarity near the base of the succession (at depth of ~10 m) but normal magnetic polarity above. ESR data of Duval et al. (2015) give ages of  $1606 \pm 187$  and  $1269 \pm 157$  ka for a sample at 14 m depth (sample ALC1202) and  $1504 \pm 229$  and  $1282 \pm 139$  ka for a sample from the upper part (depth of 4 m) of the sequence (sample ALC1201). Duval et al. (2015) consider that the most reliable age of this terrace is  $1276 \pm 104$  ka.

#### 3.2.2.3 Aragón terrace

The highest Aragón river terrace forms a ~25 km-long pedimentation surface (T1), slightly dipping (slope ca. 0.3%) toward the Ebro river to the south. This terrace T1 surface splits into four remnant pieces from north to south and is situated ~140 m above the Aragón river. Lower T2 to T7 terrace levels are deeply entrenched in the Aragón valley contrary to T1.

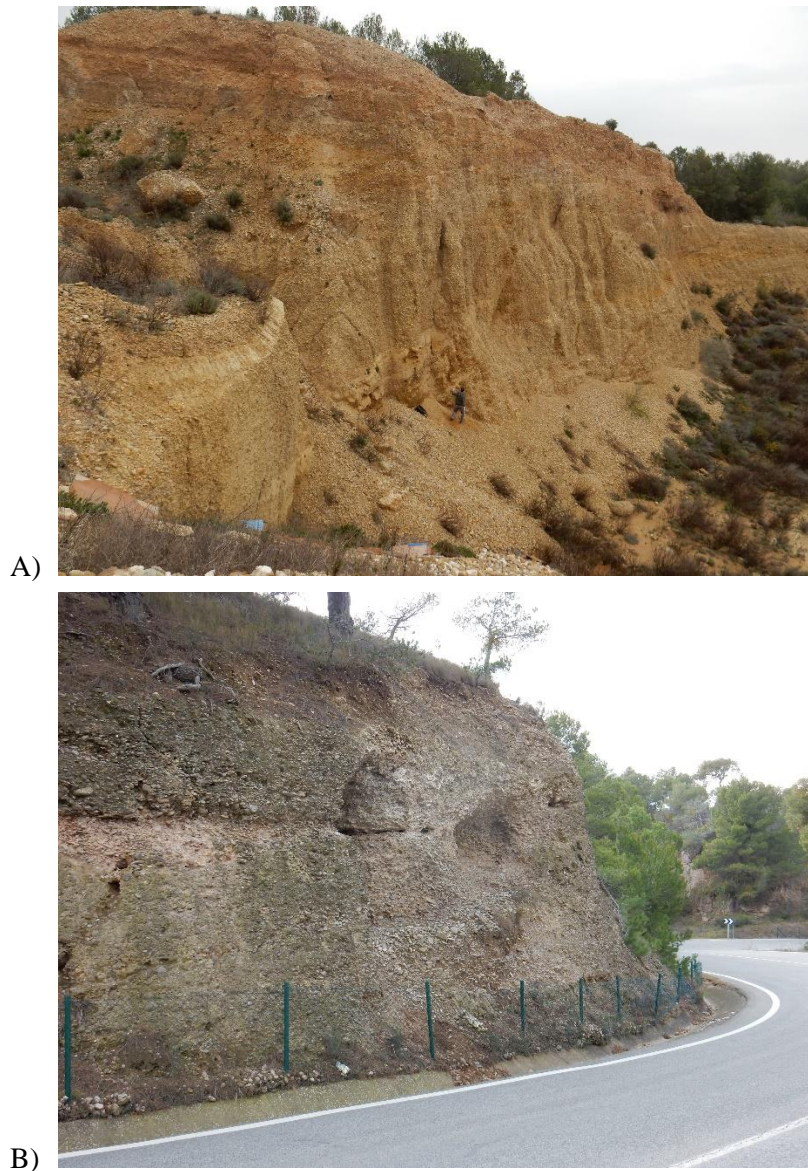


**Figure 4. TARA0 (A, -1.60158°E, 42.19839°N, 395 m) and TARA2 (B, -1.419875°E, 42.38064°N, 466 m) sampling sites.**

Two samples have been collected on this surface (A terrace level, see the following). The first sampling site (TARA0, -1.60158°E, 42.19839°N, 395 m) is located on the southernmost remnant and corresponds to a quarry, to the NNW of the Arguedas locality. It is characterized by >20 m of gravels with intercalations of sandy channels. The top (>1m) appears highly cemented by calcrete. We collected five samples from rounded quartz pebbles to sand for burial dating, at ~20 m depth (TARA0, Figure 4). The second sampling site (TARA2, -1.419875°E, 42.38064°N, 466 m) is located on the northernmost remnant, on an ancient quarry, NE of the locality of Carcastillo. The top is highly cemented by calcrete, up to ~1m depth. We collected 5 pebbles of sandstone and quartz at ~9m depth for burial dating (TARA2, Figure 4).



#### 3.2.2.4 Ebro terrace

The highest preserved terrace record of the Ebro river (T1), located between Logroño to the west and Calahorra to the east, is largely affected by erosion and shows important alteration and soil development. Terrace T1 is situated at ~200 m above the active Ebro channel (likely B terrace level, see the following). We collected 5 pebbles of quartz (TEBR2, -2.207328°E, 42.40442°N, 504 m, Figure 4) at ~10 m depth for burial dating.

#### 3.2.2.5 Najerilla terrace

The Najerilla river is a tributary of the Ebro whose headwaters are located in the Iberian Chain. The highest terrace record in the vicinity of the Najerilla river corresponds to a staircase of four distinct terraces, characterized by a slightly NW dipping (slope ca. ~0.6%). The lowest level (T4) is the most extensive (~10 km large), the highest (T1) only show a limited remnant (~700 m large).

Terrace T1 is situated at ~245 m above the Najerilla active channel (a priori corresponding to A or B terrace level, see the following). Field observations indicate important surface erosion on the top of the terrace and soil development. We collected 5 samples of quartz and sandstone pebbles at ~7.5 m depth for burial dating (TOJA1, -2.775386°E, 42.461922°N, 701 m).

### 3.2.3 Laboratory analyses and age calculations

All the samples were processed at CEREGE following standard procedures (cf. Braucher et al., 2015). They were measured at ASTER AMS (Table 1; Arnold et al., 2010).

**Table 1. Measured  $^{10}\text{Be}$  and  $^{26}\text{Al}$  concentrations.**

Sample	Mass Quartz	Spike $^9\text{Be}$	N $^{10}\text{Be}$	Measured $^{10}\text{Be}/\text{Be}$	uncertainty measure +blank	$^{10}\text{Be}$	+/-	$^{27}\text{Al}$	+/-	N $^{26}\text{Al}$	Measured $^{26}\text{Al}/^{27}\text{Al}$	uncertainty measure	$^{26}\text{Al}$	+/-	$^{26}\text{Al}/$ $^{10}\text{Be}$	+/-	
	g	at			%	at/g		at				%	at/g				
TSEGI-015	20.70	2.029E+19	6.040E+16	202	1.05E-12	8.95	1026 581	92 269	1.108E+18	1.507E+15	1183	4.86E-12	3.13	5 386 443	168 759	5.25	0.50
TSEGI-050	8.99	2.035E+19	6.058E+16	150	4.84E-13	8.26	1 087 814	90 624	1.116E+19	1.101E+17	95	8.74E-14	10.33	975 482	101 178	0.90	0.12
TSEGI-075	22.16	2.030E+19	6.044E+16	Not measurable				1.004E+18	1.668E+15	138	3.41E-12	10.61	3 419 316	362 985			
TSEGI-110	15.36	2.038E+19	6.066E+16	1208	4.62E-13	3.32	608 128	20 466	1.997E+18	3.046E+15	488	1.57E-12	5.04	3 131 287	157 833	5.15	0.31
TSEGI-138	22.10	2.035E+19	6.057E+16	Not measurable				2.398E+18	1.833E+15	407	9.19E-13	5.09	2 204 089	112 214			
TSEGI-300	21.79	2.037E+19	6.065E+16	158	9.75E-14	8.05	87 476	7 382	2.991E+18	3.160E+14	131	1.68E-13	8.81	500 990	44 155	5.73	0.70
TSEGI Enf. 1	5.73	2.030E+19	6.043E+16	17	2.62E-14	25.54	78 773	23 885	1.114E+19	2.425E+15	11	1.54E-14	31.41	171 606	53 895	2.18	0.95
TSEGI Enf. 2	20.51	2.034E+19	6.055E+16	20	1.05E-13	22.88	100 670	23 952	5.625E+18	2.487E+16	61	6.41E-14	12.86	360 284	46 346	3.58	0.97
TSEG2-016	20.50	2.039E+19	6.071E+16	1224	1.44E-12	3.25	1 426 290	46 722	2.272E+18	9.221E+14	1174	2.89E-12	3.23	6 567 168	212 433	4.60	0.21
TSEG2-040	18.51	2.036E+19	6.059E+16	767	7.60E-13	3.81	831 022	31 947	5.239E+18	1.343E+16	534	7.93E-13	4.48	4 152 099	186 321	5.00	0.30
TSEG2-100	20.09	2.037E+19	6.064E+16	293	5.45E-13	6.30	548 576	34 870	7.705E+18	1.886E+16	264	3.11E-13	6.26	2 396 931	150 230	4.37	0.39
TSEG2-130	22.28	2.036E+19	6.060E+16	331	4.74E-13	5.93	429 618	25 738	2.528E+18	9.145E+15	915	8.12E-13	3.53	2 052 626	72 889	4.78	0.33
TSEG2-180	20.08	2.039E+19	6.069E+16	47	3.48E-13	15.47	349 487	54 713	2.406E+18	3.713E+15	229	5.21E-13	6.71	1 253 418	84 116	3.59	0.61
TSEG2-380	20.69	2.034E+19	6.053E+16	45	2.10E-13	14.96	202 286	30 856	3.440E+18	1.484E+16	79	1.10E-13	11.51	378 538	43 589	1.87	0.36
TEBR2 enf. 1 A	20.68	2.034E+19	6.055E+16	835	3.29E-13	3.67	319 513	11 931	3.197E+18	8.458E+15	248	3.38E-13	6.89	1 079 230	74 443	3.38	0.26
TEBR2 enf. 1 B	20.23	2.037E+19	6.062E+16	277	1.12E-13	6.13	108 276	6 938	4.333E+18	2.008E+16	155	1.47E-13	8.12	638 458	51 898	5.90	0.61
TEBR2 enf. 1 C	21.05	2.035E+19	6.058E+16	308	1.77E-13	6.15	167 407	10 572	4.394E+18	4.504E+16	136	1.40E-13	8.65	613 864	53 489	3.67	0.39
TEBR2 enf. 1 D	20.23	2.041E+19	6.077E+16	273	1.25E-13	6.26	122 053	7 945	4.819E+18	1.666E+16	155	1.54E-13	9.08	741 854	67 397	6.08	0.68
TEBR2 enf. 1 E	21.67	2.039E+19	6.069E+16	396	1.78E-13	5.38	163 515	9 038	3.997E+18	1.135E+16	100	1.65E-13	10.07	660 776	66 547	4.04	0.46
TALC1 Enf. 1 A	20.45	2.039E+19	6.069E+16	69	5.49E-14	12.72	50 751	7 005	2.873E+18	9.242E+15	84	1.01E-13	10.97	290 656	31 905	5.73	1.01
TALC1 Enf. 1 B	20.87	2.040E+19	6.074E+16	82	9.62E-14	11.70	90 181	11 038	4.102E+18	1.739E+16	25	5.37E-14	20.79	220 174	45 793	2.44	0.59
TALC1 Enf. 1 C	21.60	2.040E+19	6.073E+16	24	6.84E-14	20.45	60 872	13 238	1.468E+18	1.276E+15	61	1.52E-13	15.11	223 414	33 760	3.67	0.97
TALC1 Enf. 1 F	20.60	2.038E+19	6.065E+16	99	8.63E-14	12.36	81 433	10 584	4.713E+18	3.363E+16	30	6.53E-14	18.29	307 716	56 337	3.78	0.85
TOJA1 Enf. 1 A	22.17	2.035E+19	6.057E+16	189	1.35E-13	7.38	119 890	9 148	3.300E+18	5.844E+15	146	1.86E-13	8.36	613 540	51 284	5.12	0.58
TOJA1 Enf. 1 B	12.11	2.039E+19	6.068E+16	194	7.63E-14	7.28	121 779	9 458	1.929E+18	8.640E+14	70	2.67E-13	13.46	515 189	69 368	4.23	0.66
TOJA1 Enf. 1 C	14.49	2.038E+19	6.067E+16	244	7.94E-14	6.52	106 127	7 373	4.332E+18	1.446E+16	118	1.40E-13	9.28	606 021	56 266	5.71	0.66
TOJA1 Enf. 1 D	16.50	2.041E+19	6.076E+16	1205	3.82E-13	3.22	467 256	15 310	3.999E+18	4.716E+15	414	5.19E-13	5.05	2 073 744	104 745	4.44	0.27
TOJA1 Enf. 1 E	18.79	2.043E+19	6.082E+16	132	1.72E-13	8.79	183 093	16 503	3.031E+18	2.391E+15	21	1.26E-13	23.75	381 067	90 495	2.08	0.53
TARA0 enf. 1 A	5.97	2.038E+19	6.066E+16	61	1.64E-14	14.04	42 544	8 334	3.711E+18	1.053E+16	11	3.43E-14	30.17	127 392	38 440	2.99	1.08
TARA0 enf. 1 B	23.00	2.047E+19	6.093E+16	108	6.30E-14	10.89	52 499	6 146	1.951E+18	4.376E+15	71	7.98E-14	11.92	155 627	18 561	2.96	0.50
TARA0 enf. 1 D	7.39	2.062E+19	6.137E+16	32	2.92E-14	17.72	70 297	14 592	6.034E+18	5.085E+15	17	2.68E-14	24.28	161 699	39 263	2.30	0.73
TARA2 enf. 1 A	22.07	2.045E+19	6.088E+16	120	1.22E-13	10.58	109 834	12 039	4.077E+18	2.841E+16	57	1.21E-13	13.73	493 236	67 810	4.49	0.79
TARA2 enf. 1 C	8.53	2.038E+19	6.068E+16	34	3.69E-14	17.19	78 582	15 264	5.619E+18	3.179E+15	16	4.10E-14	25.03	230 377	57 656	2.93	0.93
TARA2 enf. 1 D	4.11	2.044E+19	6.086E+16	67	3.22E-14	12.28	140 468	20 071	9.166E+18	8.460E+15	14	3.11E-14	27.75	285 331	79 194	2.03	0.63
Process blank		2.026E+19	6.032E+16	25	3.97E-15	20.04		2.253E+19	4.592E+16	0	0.00E+00	$\infty$					

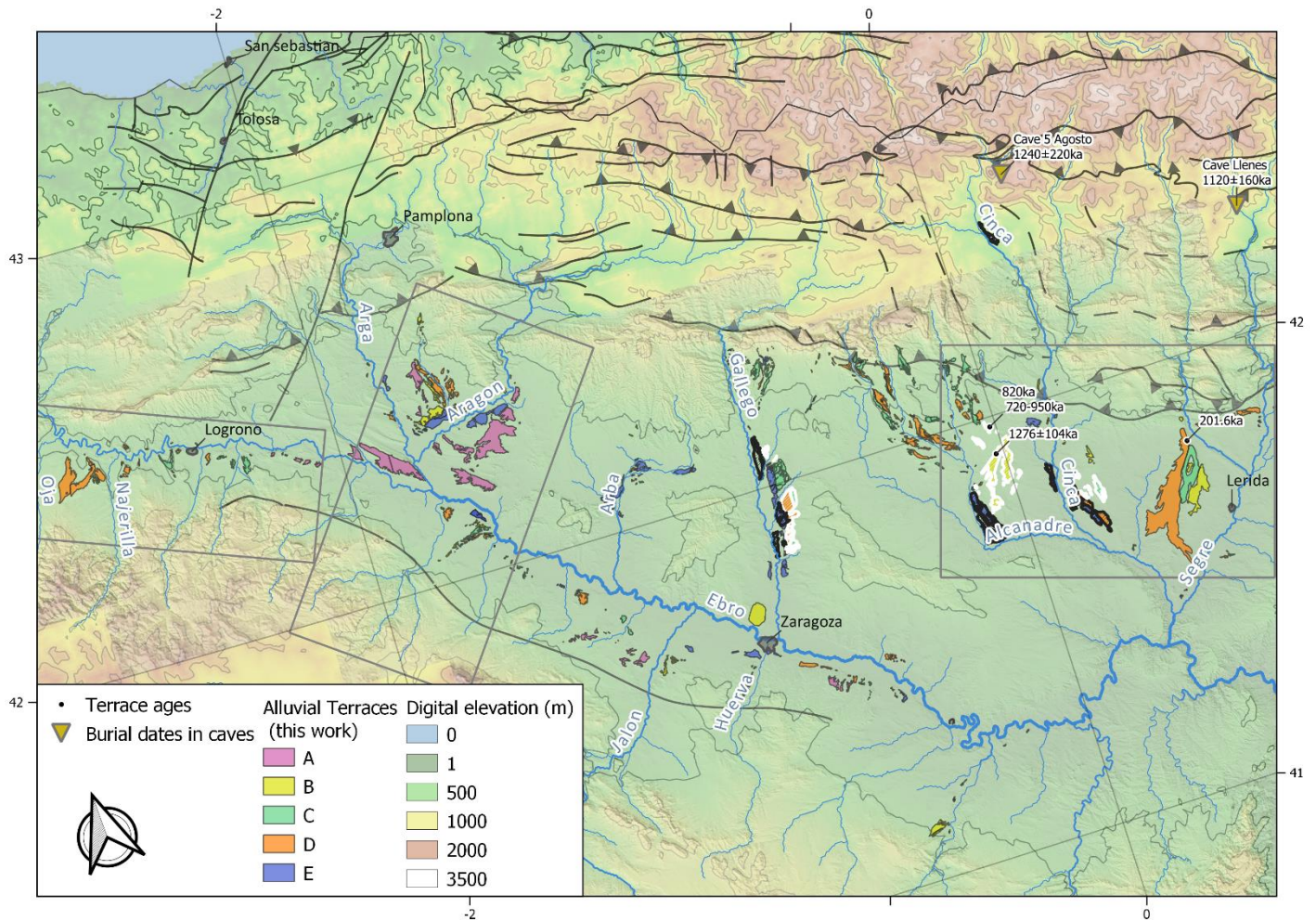


**Figure 5.** Map of the uppermost terrace record (levels A-E) in the Ebro Basin. The background corresponds to elevation. The topmost terraces are shown with the available dates for them, both from the literature and from this study. Two burial ages from Genti (2015) are mentioned: they may be related to these topmost terraces. Rectangles figure zooms of this map; they can be found in Figure 6. The produced shapefile is freely available on Zenodo ([doi:10.5281/zenodo.4721256](https://doi.org/10.5281/zenodo.4721256)).

## 4 Results

Mapping and homogenization of terrace sequences resulted in the morphological maps presented in Figure 5 and Figure 6. The mapping is comprehensive for the highest levels from A to D. The terraces corresponding to level E have been mapped where they represent an important reference in the establishment of the sequence (e.g. along the Gállego or Aragón rivers, Figure 5 and Figure 6).

We recognize the highest, oldest terrace level, labelled “A”, in the upper Ebro and Aragón valleys (Figure 5 and Figure 6). This level A constitutes probably the uppermost terrace remnants, sparsely remaining along the Ebro valley, lying more than 200 m above the current river (Figure 7a). This level is deformed near the confluence between the Aragón and Ebro rivers, suggesting it is much older than the subsequent ones. “B”, “C”, and “D” levels have been defined following the three levels identified on the interfluvium between the Noguera Rigaborçana and the Cinca rivers (Alberto et al., 1983; Stange et



al., 2013a; Lewis et al., 2017) (Figure 5 and Figure 6). Remnants of last level “D” are not parallel to the current river network and lie generally ~100 m over the current rivers (Figure 7). “E” is a usually extensive level, usually lying 40-60 m above current river courses (Figure 5 and Figure 6); it corresponds to Qt4 of Lewis et al. (2017).

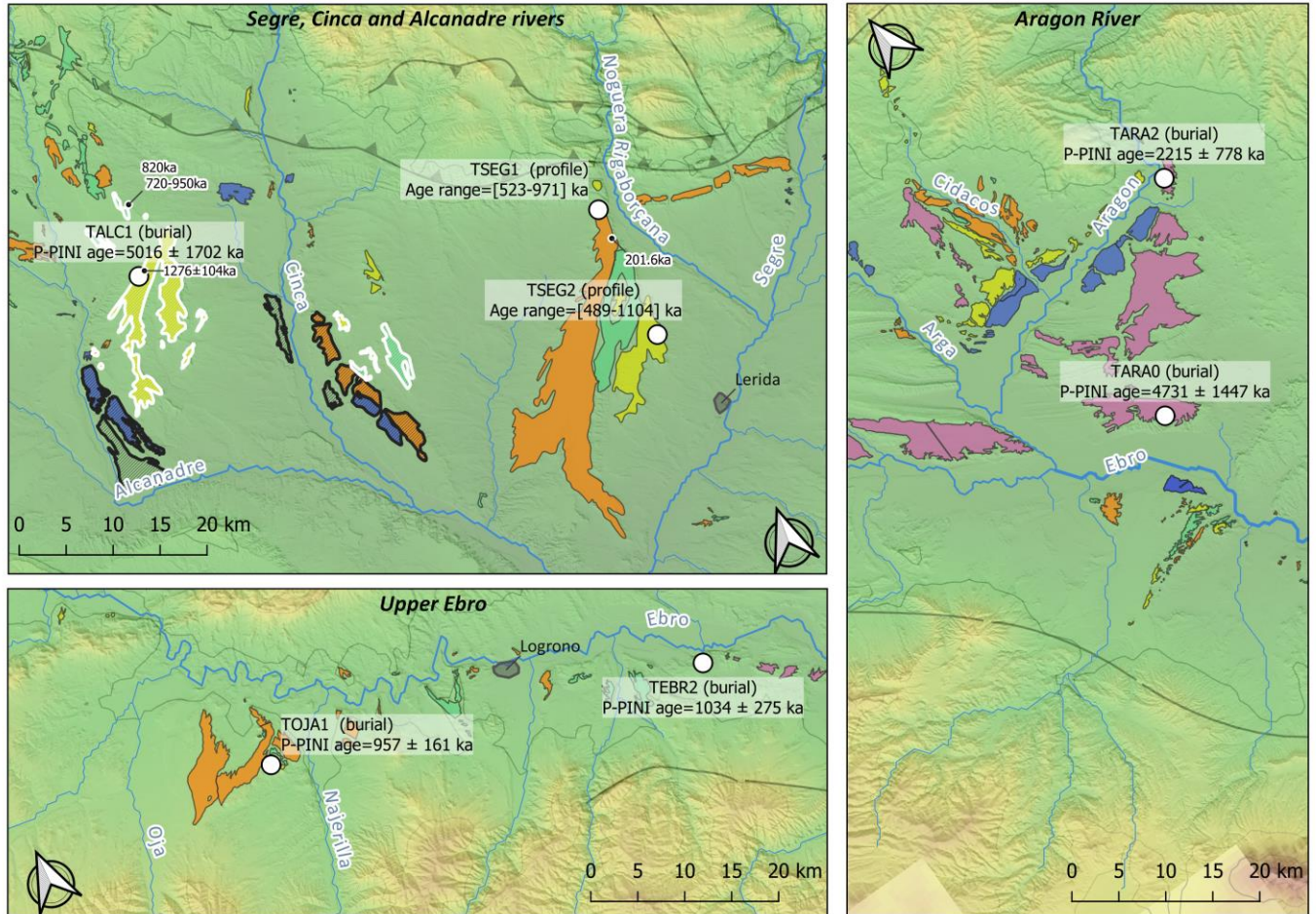


**Figure 6. Zooms of Figure 5 for places of interest discussed in this work. Same legend as Figure 5.**

#### 4.1 Dating results

For TSEG1, eight samples have been measured (Table 1 and Figure 8). Two  $^{10}\text{Be}$  Concentrations cannot be measured (Table 1). The  $^{26}\text{Al}$  concentration of the point at 50 cm depth is probably erroneous (it is 3 to 6 times less than the neighboring samples, Table 1) and has been discarded.  $^{10}\text{Be}$  and  $^{26}\text{Al}$  profiles lead to best age estimates of 693 ka (most probable age range 523-1095 ka), and, 422 ka (most probable age range 400-971 ka), respectively (Table 2). The profiles indicate that erosion rates are most probably less than 1 m/Ma, and certainly less than 2.1 m/Ma (Table 2). The overlap of  $^{10}\text{Be}$  and  $^{26}\text{Al}$  results defines a common range of 523-971 ka for TSEG1 (Figure 5 and Figure 6).

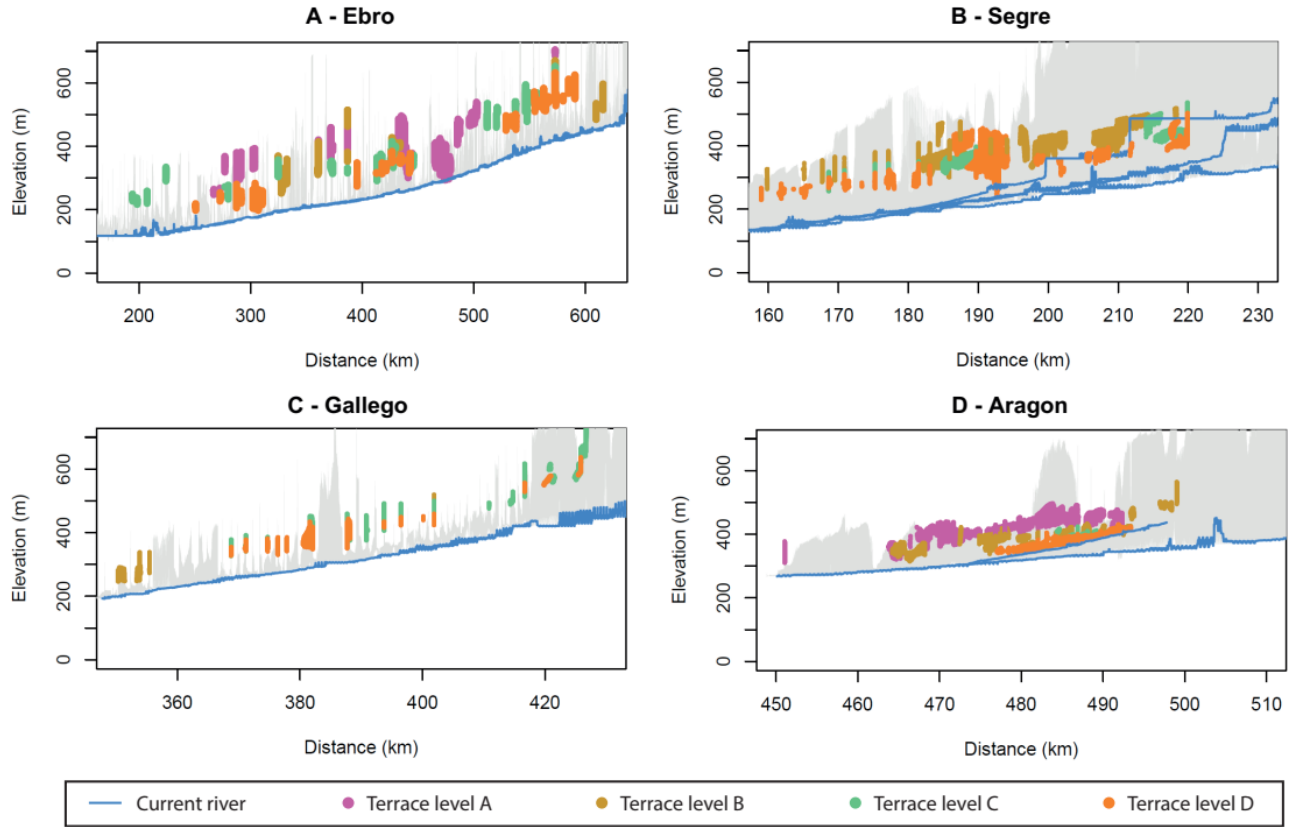


**Figure 7.** Elevation vs. distance profiles for the main river systems and their terraces. Grey: elevation in 10 km-large buffer (area within 10 km of the river) around the river trace (cf. Figure 1). The topmost terraces are shown as color dots. The color code is a function of the unified sequence defined in the results part (cf. Figure 5). The panels stand for: (A) the Ebro main stream, (B) the Segre and tributaries, (C) the Gállego valley and (D) the Aragón and Cidacos valleys. The x-axis is the distance to the Ebro mouth.

**Table 2.** Input parameters and results of cosmogenic depth profile inversions (for more details, see Supplementary Material Table S2 and Figure S2).

	TSEG1		TSEG2	
	<sup>10</sup> Be	<sup>26</sup> Al	<sup>10</sup> Be	<sup>26</sup> Al
<b>Inputs</b>				
Age range (ka)	400-1400		200-2000	
Erosion rate max (m/Ma)	5		2.5	
Erosion threshold (m)	2		4	
Inheritance max (at/g)	80000	360000	250000	400000
<b>Results</b>				
Best age (ka)	693	422	532	435
Age range (ka)	523-1095	400-971	489-1961	374-1104
Common age range (ka)	523-971		489-1104	
Erosion rate max (m/Ma)	1	2.1	1.8	1.6
Inheritance max (at/g)	44000	300000	24000	300000



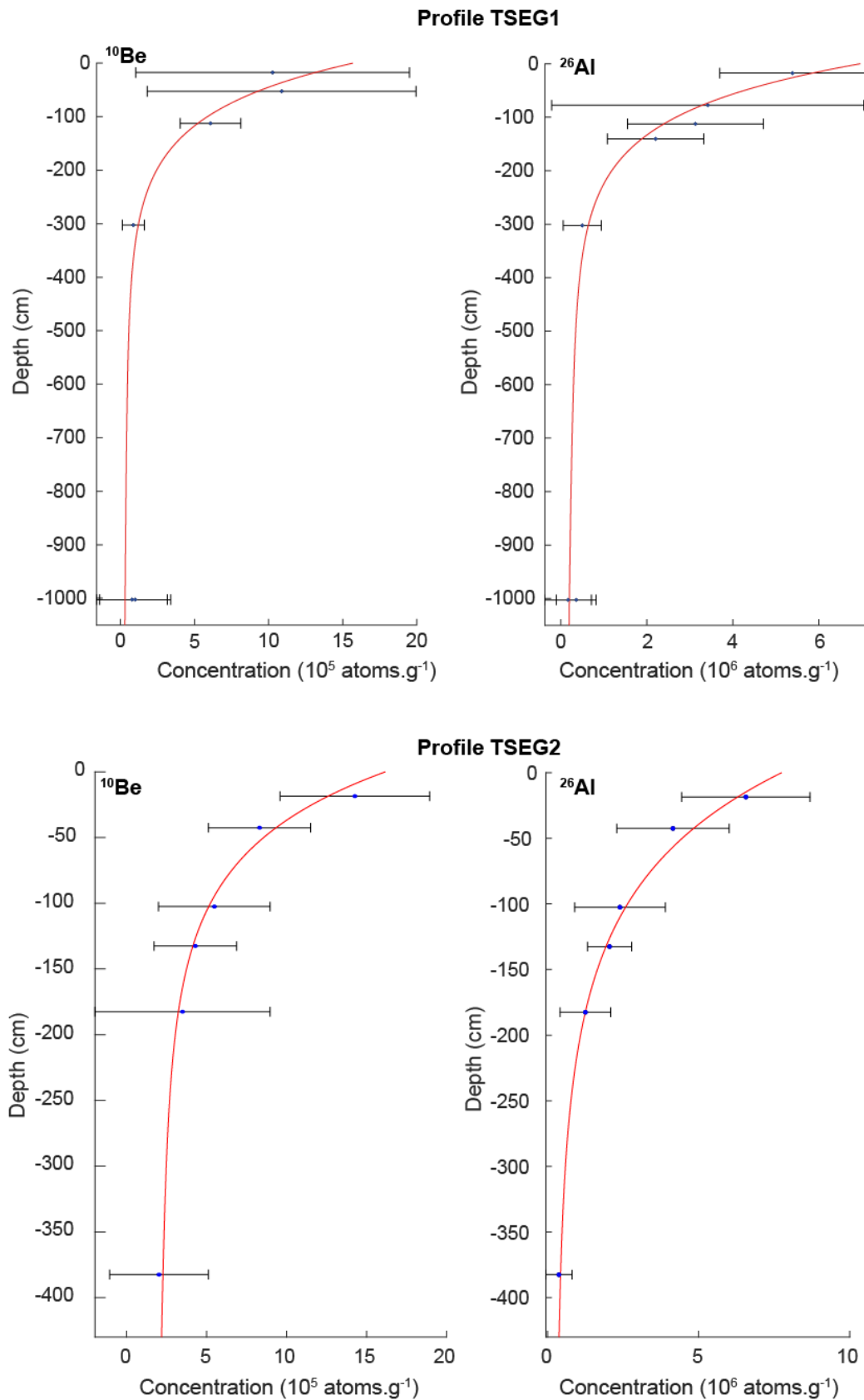


**Figure 8. Cosmogenic nuclide concentration profiles TSEG1 et TSEG2 (best profile).**

Six TSEG2 samples have been measured (Figure 8).  $^{10}\text{Be}$  and  $^{26}\text{Al}$  profiles lead to best age estimates of 532 ka (most probable age range 489-1961 ka), and, 435 ka (most probable age range 374-1104 ka),

respectively (Table 2). Erosion rates are most probably less than 1.8 m/Ma (Table 2). The overlap of  $^{10}\text{Be}$  and  $^{26}\text{Al}$  results defines a common range of 489-1104 ka for TSEG2 (Figure 5 and Figure 6).

For TARA0, P-PINI indicates a best terrace age of  $4731 \pm 1447$  ka (Table 3). For TARA2, P-PINI computed  $2215 \pm 778$  ka (Table 3). For TEBR2, TOJA1, and TALC1, P-PINI indicates ages of, respectively,  $1034 \pm 275$  ka,  $957 \pm 161$  ka, and  $5016 \pm 1702$  ka (Table 3, Figure 5 and Figure 6). The large uncertainty for TALC1 and TARA2 comes from a low (insufficient) number of samples and that the concentrations are too similar to be well constrained by the P-PINI or Isochron method (Balco and Rovey, 2008).

**Table 3. Main burial dates from P-PINI inversion (for more information, cf. Supplementary Material).**

Site	P-PINI age (ka)	+/-
TARA0	4731	1447
TARA2	2215	778
TEBR2	1034	275
TOJA1	957	161
TALC1	5016	1702

## 4.2 Unified terrace chronology

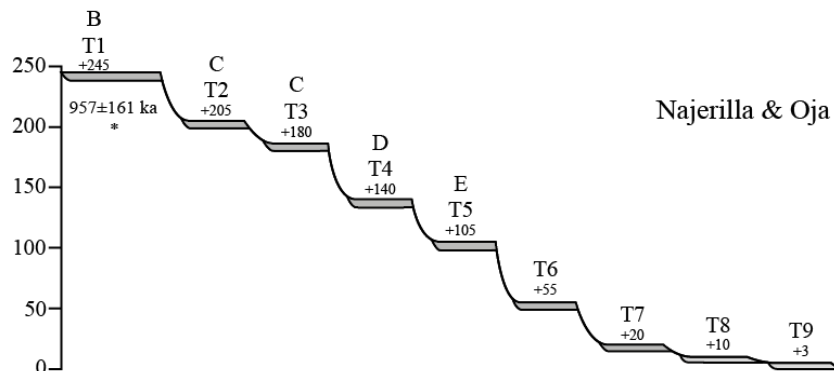
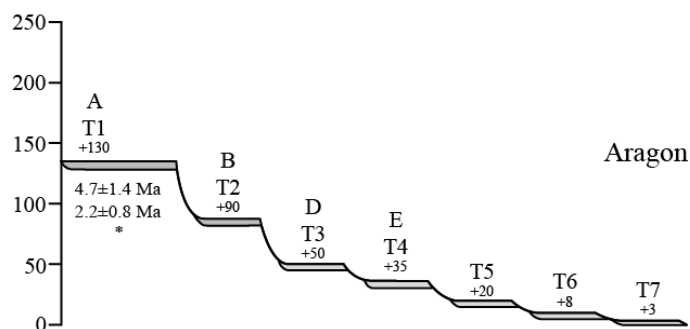
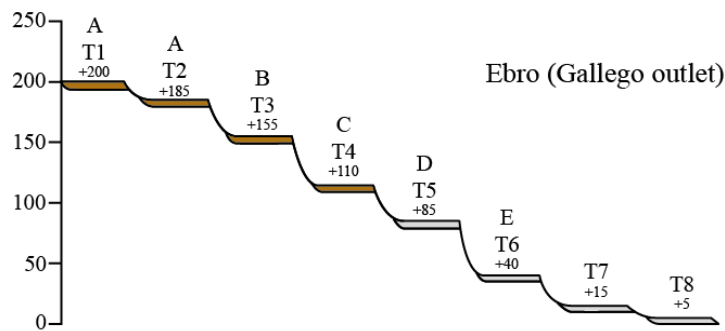
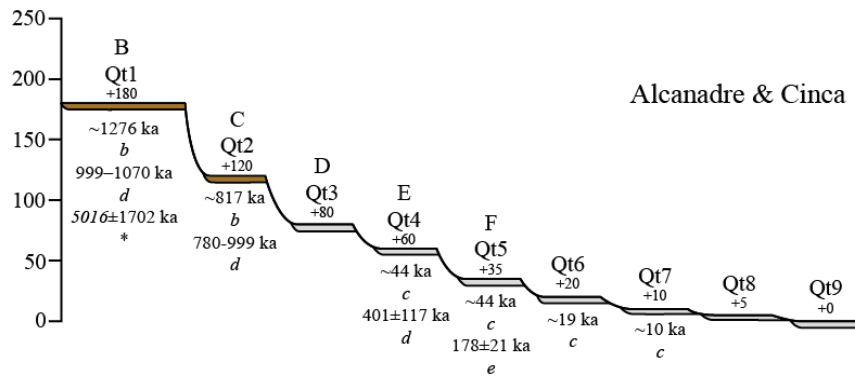
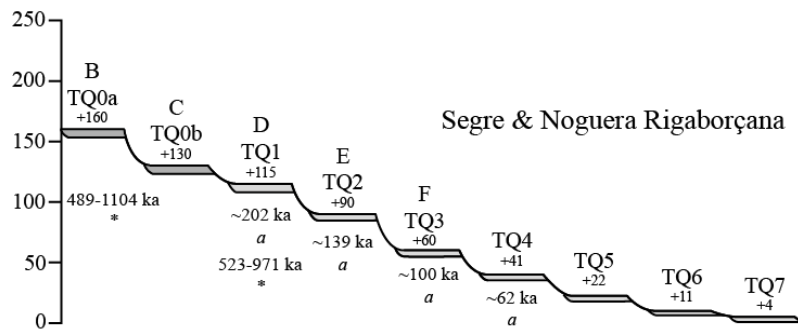
Previously, we have presented our relative terrace chronology, leading to terrace levels labelled in alphabetical order starting with A. We now analyze the absolute chronology.

Previous works mainly focused in the eastern part of the basin. In the Segre catchment, study sites from B and C levels provided inverse magnetic polarity while the magnetic polarity is normal for sites from D (Figure 9)(Calle et al., 2013; Lewis et al., 2017). ESR dates proposed are  $1276 \pm 104$  ka and  $817 \pm 68$  ka (Duval et al., 2015), for terraces mapped as B and C, respectively (Figure 9). Our P-PINI burial age for B at TALC1 is  $5016 \pm 1702$  ka appears erroneous maybe because it is poorly constrained, probably because of too little data. Our dates from cosmogenic depth profiles are 489-1104 ka for B (TSEG2) and 523-971 ka for D (TSEG1, Figure 6 and Figure 9). Besides, Lewis et al. (2017) proposed an age of  $401 \pm 117$  ka for the next terrace level (E, Figure 9).

Towards the west, around the Aragón valley, even if it is tempting to correlate the topmost terrace of Bomer (1979) with the B level, the topmost terrace is likely to be much older, as emphasized by the old cosmogenic nuclide ages ( $>2$  Ma) found for TARA0, TARA2 upstream from the confluence from the Aragón and Ebro rivers (Figure 5, Figure 6 and Figure 9). This antiquity is further confirmed by the deformation of this terrace level, whereas the lower levels, including the well-developed E level in the area, are not deformed (see Casas et al., 1994 and the corresponding 1:50000 geological map).

**Table 4. Synthesis of terrace level ages, from this study and literature. \* Inverse weighted average; when age range, we suppose a normal distribution. † With or without related karst data, average ~1150 ka; an uncertainty of 150 ka satisfactorily encompasses the various estimates. ‡ Average with uncertainty encompassing the various estimates. ◇ Value satisfying both paleomagnetic constraints and the age estimates for C and E.**

Terrace level	Median elevation above current river (m)	Published age	Method	Reference	This study	Conclusions/ Adopted age
A	210 (Zaragoza area) 130 (Aragón)				TARA0: 4731±1447 ka (P-PINI) TARA2: 2215±778 ka (P-PINI) Mean*: 2780 ± 690 ka	2800±700 Ma
B	150-180 (North-East)	1276±104 ka	ESR	Duval et al. 2017	TALC1: 5016±1702 ka (P-PINI)	
	140 (Ebro between Zaragoza and Aragón)	[999-1070] ka	Tentative age from paleomagnetic data	Lewis et al. 2017	TEBR2: 1034±275 ka (P-PINI)	
	90 (Aragón)	>780 ka	Paleomagnetism	Lewis et al. 2017	TOJA1: 957±161 ka (P-PINI)	1150±150 ka†
	200 (Upper Ebro)				TSEG2: [489-1104] ka (profile) Mean*: 970 ± 130 ka	
C	140 (North-East)	817±68 ka	ESR	Duval et al. 2017		
	130 (Gállego)	[780-999] ka	Tentative age from paleomagnetic data	Lewis et al. 2017		
	115 (Ebro between Zaragoza and Aragón)	>780 ka	Paleomagnetism	Lewis et al. 2017		850±70 ka‡
	170 (Upper Ebro)					
D	100 (North-East)	<780 ka	Paleomagnetism	Lewis et al. 2017	TSEG1: [523-971] ka (profile)	
	100 (Gállego)	~780 ka	Paleomagnetism	Calle et al. 2013		
	80 (Ebro downstream Zaragoza)					650±130 ka◇
	90 (Ebro between Zaragoza and Aragón)					
	130 (Upper Ebro)					
E	80 (North-East)	401±117 ka	Compilation of various data	Lewis et al. 2017		
	70 (Gállego)					
	50 (Ebro between Zaragoza and Aragón)					400±120
	35-40 (Aragón)					



**Literature data**  
*a* Stange *et al.*, 2013  
*b* Duval *et al.*, 2015  
*c* Calle *et al.*, 2013  
*d* Lewis *et al.*, 2017  
*e* Lewis *et al.*, 2017  
 \* This study (data)  
 Inverse magnetic polarity (c,d)

**Proposed ages**  
 (compilation, this study)  
**A** 3.1 ± 0.7 Ma  
**B** 1.1 ± 0.15 Ma  
**C** 850 ± 70 ka  
**D** 650 ± 130 ka  
**E** 400 ± 120 ka

**Figure 9. Terrace elevation (above current river course) and labels from the literature and our homogenization scheme (A to F); maroon-colored terraces represent pre- Brunhes/Matuyama transition (780 ka), when measured. Published and new dates are indicated, as well as our proposed chronology.**

The A level was not previously dated. It corresponds to two sites from the present study (TARA0 and TARA2). The P-PINI dates for these two sites are quite different but both agree on a fairly old age. None of the dates are very reliable due to the low number of data. Since we cannot choose between the two, we adopt the mean age of  $\sim 2.8 \pm 0.7$  Ma (Table 4). We note, however, that this age represents well the samples TARA0-B, TARA0-D, TARA2-C and TARA2-D (Supplementary Material, Figure S10 and S13). The B level was deposited with inverse magnetic polarity (Calle et al., 2013; Lewis et al., 2017), and dated at  $\sim 1.3$  Ma (Duval et al., 2017). TSEG2, sampled from this level, yields an age of 489-1104 ka, by a cosmogenic profile method (Figure 9). Also, TOJA1 ( $960 \pm 160$  ka), in the upper reaches of the Ebro main valley, could correspond to this level. We had some doubt regarding which terrace level, A or B, TEBR2 belongs to. Its P-PINI age of  $1.03 \pm 0.27$  Ma clearly falls in the range of the level B (Table 4). Consequently, and considering B is older than C (see below), we regard an age of  $1.15 \pm 0.15$  Ma to be likely for this level B (Table 4). The age of C, the next level, is constrained by an inverse magnetic polarity (Lewis et al., 2017), and one ESR estimate of  $\sim 0.8$  Ma (Duval et al., 2017). Its likely age is  $850 \pm 70$  ka after our analysis (Figure 9 and Table 4). The terrace level D mostly displays a normal magnetic polarity (Calle et al., 2013; Lewis et al., 2017). We estimate an age of 523 to 971 ka (TSEG1) from our cosmogenic depth profile that is much older than the estimate by Stange et al. (2013a). Together with the C and E terrace dates, which must be older and younger, respectively, we propose an age of  $\sim 650 \pm 130$  ka for this D level (Figure 9 and Table 4). Finally, terrace E has been dated to be  $401 \pm 117$  ka (Lewis et al., 2017) (Figure 9). We summarize the absolute age constraints on Table 4: we estimate ages for terraces A, B, C, D, E to be  $2.8 \pm 0.7$  Ma,  $1.15 \pm 0.15$  Ma,  $850 \pm 70$  ka,  $650 \pm 130$  ka and  $400 \pm 120$  ka, respectively (Figure 9 and Table 4).

## 5 Discussion

The youngest sediments of the endorheic stage preserved in the Ebro Basin are late Miocene (see Section 2.2) lacustrine and fluvial deposits (Pérez-Rivarés et al., 2002, 2004; Garcia-Castellanos et al., 2003; Garcia-Castellanos, 2006; Larrasoña et al., 2006; Vázquez-Urbez et al., 2013; Calvet et al., 2020). They are observed 500 m above the Ebro river course, and have possibly been covered by younger sediments now eroded (Garcia-Castellanos and Larrasoña, 2015). The subsequent erosion of the Ebro basin was limited and affected mostly the Miocene deposits that are currently preserved in the form of alluvial deposits but also pediments. Plio-Pleistocene alluvial remnants are mostly terraces found along (and parallel to) the main rivers in valleys within the basin. Some of these remnants are lying on interfluvial crests between the main valleys. Among them, good examples are represented by terraces between the Noguera Rigaborçana and the Cinca valleys (levels B, C, and D). These uppermost terraces argue for a



mobile fluvial network while the lowermost ones reflect river entrenchment without significant lateral mobility. This change in fluvial behavior seems to have occurred at the time of deposition of terrace level D, shortly after the Brunhes-Matuyama transition at 780 ka (Figure 9). This agrees with the change in fluvial style at the Mid-Pleistocene Transition proposed by Sancho et al. (2016).

## 5.1 Terrace chronology

The proposed chronology for terraces A, B, C, D, E is  $2.8 \pm 0.7$  Ma,  $1.15 \pm 0.15$  Ma,  $850 \pm 70$  ka,  $650 \pm 130$  ka and  $400 \pm 120$  ka, respectively (Figure 9). These dates are the result of a compilation of ages obtained with various methods (Table 4): ESR, paleomagnetism, cosmogenic nuclide depth profiles, and cosmogenic nuclide burial ages from the isotope pair ( $^{10}\text{Be}$ ,  $^{26}\text{Al}$ ) (in caves and in terraces through P-PINI inversion). The number and quality of data for each level of terrace are variable. For example, paleomagnetism only indicates if the terrace level is younger or older than the Brunhes-Matuyama transition (780 ka). Also, after our own experience, cosmogenic nuclide depth profiles are not accurate when the ages exceed 500 ka, and can be significantly altered by terrace post-abandonment surface evolution. For example, the ages computed from depth profiles published in Stange et al. (2013a) are probably underestimated (see also Delmas et al., 2018; Delmas, 2019). Similarly, our own depth profiles, which do not give an unequivocal result, probably tend to underestimate the ages, possibly because of a recent acceleration of erosion. The  $2.8 \pm 0.7$  Ma for the level A is not very good because the two estimates on the uppermost Aragón terrace largely differ (TARA0 at  $4730 \pm 1450$  ka and TARA2:  $2210 \pm 780$  ka). The level B benefits from a large number of dating attempts. Its P-PINI cosmogenic burial dates agree with ESR (except for TALC1) and an inverse magnetic polarity. The age suggested by our depth profile data (TSEG-2) is a bit younger than the average age of  $\sim 1150$  ka calculated for level B but is older than the age proposed by Stange et al. (2013a). Level C delivered only two but overlapping pieces of information, making it reliable: an inverse magnetic polarity (Lewis et al., 2009) and an ESR age of  $817 \pm 68$  ka (Duval et al., 2017). On level D, we produced a depth-profile cosmogenic age, which, despite the aforementioned caveats, and with the constraint of normal magnetic polarity, allows to restrict the range of possible ages to  $650 \pm 130$  ka.

In the nearby Arlanzon valley in the upper part of the Duero basin (location shown in Figure 1), Moreno et al. (2012) used the ESR technique to date the uppermost terraces:  $1140 \pm 130$  ka for the T3 terrace,  $780 \pm 120$  ka and  $939 \pm 100$  ka for the inverse polarity T4 terrace,  $700 \pm 100$  ka,  $600 \pm 100$  ka, and  $700 \pm 70$  ka for T5, and  $400 \pm 90$  ka, and  $370 \pm 70$  ka for T8. These ages agree well with our own estimates: the Arlanzon terraces T8, T5, T4, and T3 correlate with the Ebro Basin terraces E, D, C and B respectively (cf. Figure 1). Similarly, on the northern side of the Pyrenees, the uppermost Têt river terrace (T5) has provided two ESR dates at  $1099 \pm 179$  ka and  $1133 \pm 159$  ka (Delmas et al., 2018), again contemporaneous to B. Along the Têt river, age of T4 is still debated while the T3 terrace level below has been dated with ESR technique to be  $\sim 400$  ka ( $440 \pm 39$  ka, and  $374 \pm 47$  ka) (Delmas et al., 2018).

The Têt terraces T5 and T3 should then correspond to our B and E levels, respectively, as already noted by Delmas et al. (2018). In the Pyrenees, some karst dates fall within the age range we propose in the Ebro basin. The Llenes cave, located ~100 m above the present course of the river, and dated by  $^{26}\text{Al}/^{10}\text{Be}$  burial dating to  $1120\pm160$  ka (Genti, 2015), could certainly be correlated with level B (see Calvet et al., 2015 and refs included for the correlation between cave systems and terraces). More doubtful is Cave 5 of Agosto which has a similar age ( $1240\pm220$  ka Genti, 2015), but at a much higher elevation (800 m above the present river). Finally, it appears that the chronology of the Ebro basin shares lots of similarities with adjacent areas. We conclude that the distribution of terrace ages is a regional signal, not specific to the Ebro Basin.

We observed that rivers begin to entrench around terrace levels B to D: it marks the transition from large terraces now lying on interfluvies to sequences of young terraces developing parallel to the current river courses. On the basis of physical models (Bufe et al., 2016; Baynes et al., 2020) as well as natural systems (Bufe et al., 2017), it turns out that large terraces are produced by high channel mobility, which in turn depends on water and sediment fluxes, themselves a function of climate. As already proposed by Sancho et al. (2016), it is tempting to relate this entrenchment to climate as it has occurred during or shortly after the Middle Pleistocene Transition (MPT, 1.3 to 0.7 Ma ago). Indeed, the MPT is due to dominant orbital periodicity change from 41 ka to 100 ka (Tziperman and Gildor, 2003; Lisiecki and Raymo, 2005; Siddall et al., 2010). This led to an increase of climatic contrasts, triggering intense glacier fluctuations in the surrounding mountain ranges and controlling sediment discharge and river incisions, similar to what we observe in the Ebro Basin (Stange et al., 2013a, 2013b; Lewis et al., 2017). Our observations further suggest that before the MPT, the upper Pliocene/lower Pleistocene climate favored a mobile river network. This idea is, on the one hand, challenged by Santisteban and Schulte (2007) who claimed for a diachronous incision beginning along the Iberian rivers. On the other hand, the MPT increase in incision rates is attested all over Europe (Gibbard and Lewin, 2009). We infer that the river network has been fixed when the climate underwent larger and longer glacial/interglacial oscillations.

## 5.2 Incision: rates and significance

The incision appears to have accelerated for the last million years. In the center of the basin, around Zaragoza, the youngest endorheic sediments are currently lying at an elevation of ~700 m (Pérez-Rivarrés et al., 2002, 2004; Vázquez-Urbez et al., 2013), ~500 m above the nearby Ebro river. A and B terraces lying 200-220 m and 140 m above Ebro river, respectively. The total amount of incision is ~300 m between the Ebro Basin opening (13-7.5 Ma) and the topmost terraces A. This is a minimum, given the possibility these strata have been buried under a couple of hundreds of meters of younger sediments before being exhumed (Garcia-Castellanos and Larrasoana, 2015). Thus, in the Zaragoza area, the incision was ~40 m/Ma before 2.8 Ma then ~40 m/Ma for the period 2.8-1.15 Ma and ~120 m/Ma (x3) since then (Figure 10). Along the Aragón valley, A and B are 130 m and 90 m above the current river,

respectively: the incision rate varies from ~25 m/Ma for the period 2.8-1.15 Ma to ~80 m/Ma (x3, for uncertainties see Table S1, Supplementary material) for the last 1.15 Ma (Figure 10). We tested the robustness of these observations taking into account various ages and terrace elevation datasets presented in Figure S1 (Supplementary Material). It indicates that most of the Ebro basin rivers entrenched at a rate of 110 to 220 m/Ma. As proposed by Sancho et al. (2016), such a rate cannot have lasted for many millions of years, in agreement with a recent acceleration of incision. This analysis also confirms that incision acceleration may have occurred around 1 Ma ago, as shown by the two areas displaying old terraces: the lower Gállego and the Aragón valleys (Figure S1, Supplementary Material). In the Duero basin, Rodríguez-Rodríguez et al. (2020) documented an increase in catchment-wide denudation rate by factor of two or three (x2 to x3) since 1 to 2 Ma. However, the authors relate this acceleration to expansion of the Duero drainage network driven by long-term base-level lowering and autogenic processes rather than to a climatic signal.

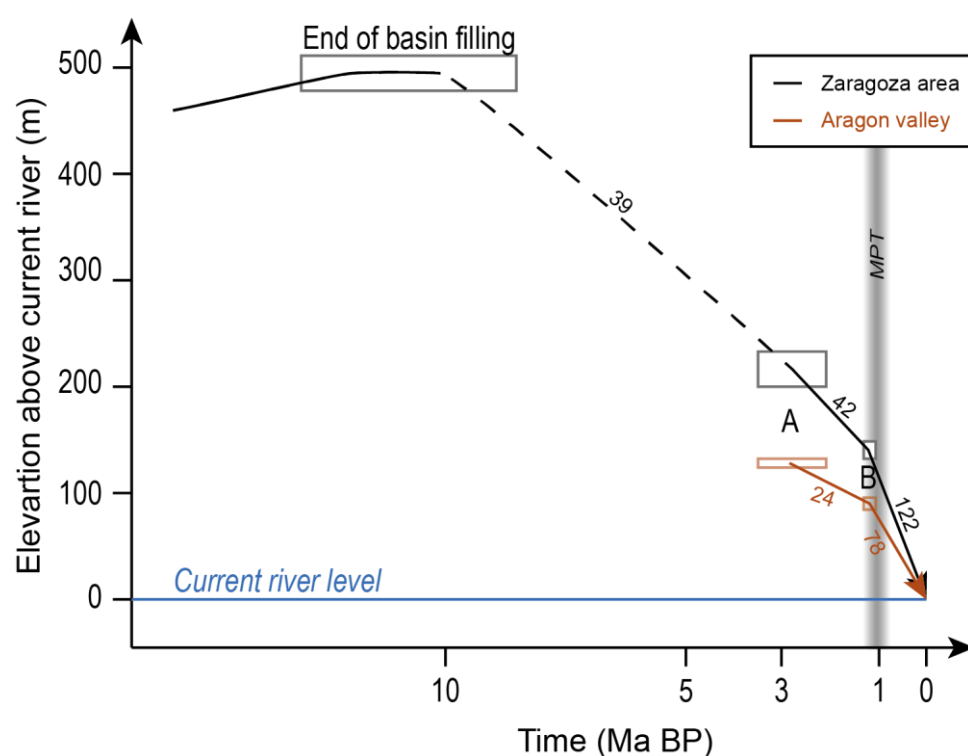


**Figure 10.** Incision in the Ebro Basin since 10 Ma in two key areas, the Zaragoza area (black) where the end of basin infilling is recorded, and the Aragón valley (brown). Rectangles figure the constraints. Numbers represent the incision rate in m/Ma. The path for the period between 10 and 3 Ma is shown with a dashed line, which figures the possibility the current topmost strata have been buried for a while (Garcia-Castellanos and Larrasoana, 2015). The Zaragoza area does not show a marked change at ~3 Ma. On the contrary, both records suggest a threefold increase in incision rates after the MPT.

We note that the incision calculated in the Zaragoza area of 500 m is possibly underestimated if the latest pre-opening sediments have been buried before exhumation (Garcia-Castellanos and Larasoana, 2015). Thus the pre-2.8 Ma period incision is (slightly?) lower than in the southern flank of the Pyrenean Axial Zone for the last 9 Ma deduced from low-temperature thermochronology (700-1600 m, equivalent

to an exhumation rate of 130-500 m/Ma, Fillon et al., 2013). This could be partly explained by the larger amount of sediments at the foot of the axial zone, where paleovalleys were filled by up to 2000 m of conglomeratic sediments now eroded (e.g. Vincent, 2001; Babault et al., 2005a; Fillon et al., 2013). It also indicates that Neogene erosion has been stronger at the foot of the Axial Zone than in the centre of the basin, which is consistent with a significant uplift of the Pyrenees relatively to the basin since 10 Ma (e.g. Conway-Jones et al., 2019; Calvet et al., 2020).

Most upper terraces developed at the outlet of Pyrenean streams when they enter into the Ebro sedimentary basin. Extensive terrace sequences developed similarly along rivers flowing from the Iberian Chain to the south. Rivers flowing mainly within the Ebro Basin, in contrast, show less extensive terrace development, as along the Arba river. In the NW of the basin, a comparison between the Cidacos and Arga rivers is enlightening: despite of small length, the Cidacos river left large terraces, while the longer nearby Arga river shows sparse terraces with little lateral extent. Maybe, as the Arga is larger, it eroded more the ancient terraces and the Cidacos terrace remnants could be conceived more like pediments? Nevertheless, it suggests that large terrace sequences are found if (i) they form large/thick surfaces, and (ii) later river mobility was not sufficient to remove them.

Terrace distribution also indicates that older terraces developed preferentially out of the basin center and from east to west (Santisteban and Schulte, 2007). In the eastern part of the basin, the absence of the topmost level A, together with the location of the lower levels on top of the interfluvies suggests that a large reshaping occurred at the Plio-Pleistocene transition. This reshaping may have produced a pediment landscape such as in the current Arba catchment (Centre-north of the basin). There, large pediments are found, in a depressed position relative to the Aragón terraces to the north-west. This is consistent with observations from other rivers of Europe for which slight incision documented during the Latest Pliocene/Early Pleistocene led to the development of wide and shallow valleys (Gibbard and Lewin, 2009). The east-west difference is also marked by a decrease of incision to the west, which could be explained by upstream incision wave migration, as recently documented in the Duero (Rodríguez-Rodríguez et al., 2020). This incision wave is currently affecting the drainage divide between the Duero and Ebro catchments (Vacherat et al., 2018; Struth et al., 2019). Hence, the large and old terraces found upstream could correspond to the smooth landscape characterizing the area before Late Pliocene/Pleistocene incision. The geomorphic processes active at this time may have been diffuse, explaining the large scatter between the ages found (cf. burial dates of TARA0, TARA2). This upstream incision wave migration is potentially enhanced by an erosional isostatic rebound more pronounced in the center and eastern part of the basin than in the western part (Garcia-Castellanos and Larrasoña, 2015). This isostatically induced rebound is due to basin unfilling but can also be caused by moderate to important denudation of the Pyrenees and Central Iberian Massif in Plio-Pleistocene times (Garcia-Castellanos and Larrasoña, 2015; Stange et al., 2016). In the center-east part of the basin, this uplift does not necessarily differ from the center of the basin to the Pyrenees foothills, explaining why terrace

levels are parallel such as for the Segre and its tributaries (Figure 7b). This observation seems to be valid also for the Gállego river (Figure 7c), despite the karstic deformation occurring in its lower reaches (Benito et al., 1998, 2000; Guerrero et al., 2008, 2013). To the west, the Aragón river terraces show a clear decreasing incision trend downstream (Figure 7e), while the trend is opposite along the upper Ebro River (e.g. the Oja/Najerilla system near the Ebro-Duero drainage divide). This trend is however not well resolved and would need additional works if we are to discuss its correlation with the post-Miocene tilt shown by lacustrine strata covering the Ebro and Duero basins (Garcia-Castellanos and Larrasoana, 2015). At a shorter time scale, incision rates significantly increased as already noted by Sancho et al. (2016). Post MPT increased erosion is likely controlled by erosion waves characterized by knickpoints migrating upstream, possibly originated at the coast as a consequence of eustatic fluctuations (e.g. Antoine et al., 2000; Crosby and Whipple, 2006; Bridgland and Westaway, 2008; Loget and Van Den Driessche, 2009). While migrating upstream, the amplitude of erosion waves could be attenuated with higher incision rates downstream as recently documented on the Duero (Rodríguez-Rodríguez et al., 2020). Hence, the more pronounced incision in the east of the basin may be driven by a position closer to the Mediterranean Sea, possibly enhanced by a Quaternary flexural erosional uplift of the entire basin up to the Catalan Coastal Range (Lewis et al., 2000; Stange et al., 2016).

## 6 Conclusion

A unified fluvial terrace chronology and mapping have been produced for the Ebro Basin. It is based on a review of ages from the literature and new cosmogenic nuclide ages obtained with the profile and P-PINI methods. From the topmost terrace downward, the terraces are labelled in alphabetical order. Terraces A, B, C, D, and E are dated to  $2.8 \pm 0.7$  Ma,  $1.15 \pm 0.15$  Ma,  $850 \pm 70$  ka,  $650 \pm 130$  ka and  $400 \pm 120$  ka, respectively, in agreement with other dated terraces in the Iberian Peninsula and around the Pyrenees. The oldest ones (A, B, and C) are extensive, testifying for wandering fluvial systems while from D to present, the network has been stabilized and is currently entrenched in 100 to 200 m-deep valleys. We therefore hypothesize that a transition occurred from mobile to localized fluvial network. We propose this transition is likely related to the Middle Pleistocene Transition (MPT, between 0.7 and 1.3 Ma), when long-period/high-intensity climate fluctuations were established in Europe. We estimate that between 2.8-1.15 Ma and present, the incision rates have tripled, from 25-40 m/Ma to 80-120 m/Ma. After the MPT, the terrace disposition also shows more important incision and basin unfilling in the east possibly enhanced by flexural rebound.

## 7 Acknowledgements

V. Zavala and J. Rat participated to the field work. We thank M. Delmas, R. Braucher, and S. Carretier for fruitful discussions. This work benefited from support and funding by OROGEN TOTAL-BRGM-

CNRS project. We thank two reviewers, M. Calvet and D. García-Castellanos, and Editor A. Teixell for their careful reading and constructive comments.

## 8 References

- Alberto, F., Gutiérrez, M., Ibáñez, M.J., Machín, J., Meléndez, A., Peña, J., and Rodríguez, J., 1983, El piedemonte pliocuaternario en el sector central pirenaico (Huesca y Lérida): *Geographica*, p. 109–126.
- Anderson, R.S., Repka, J.L., and Dick, G.S., 1996, Explicit treatment of inheritance in dating depositional surfaces using in situ  $^{10}\text{Be}$  and  $^{26}\text{Al}$ : *Geology*, v. 24, p. 47–51.
- Antoine, P., Lautridou, J.P., and Laurent, M., 2000, Long-term fluvial archives in NW France: response of the Seine and Somme rivers to tectonic movements, climatic variations and sea-level changes: *Geomorphology*, v. 33, p. 183–207.
- Arasa-Tuliesa, A., and Cabrera, L., 2018, Neogene-Quaternary onshore record in the lower Ebro river incised palaeovalley (Ebro margin, Catalan Coastal Range, NE Iberia): *Geologica Acta*, v. 16, p. 265–292, I– XII, doi:10.1344/GeologicaActa2018.16.3.3.
- Arboleya, M.-L., Babault, J., Owen, L.A., Teixell, A., and Finkel, R.C., 2008, Timing and nature of Quaternary fluvial incision in the Ouarzazate foreland basin, Morocco: *Journal of the Geological Society*, v. 165, p. 1059–1073, doi:10.1144/0016-76492007-151.
- Arnold, M., Merchel, S., Bourlès, D.L., Braucher, R., Benedetti, L., Finkel, R.C., Aumaître, G., Gott dang, A., and Klein, M., 2010, The French accelerator mass spectrometry facility ASTER: Improved performance and developments: *Nuclear Instruments and Methods in Physics Research Section B: Beam Interactions with Materials and Atoms*, v. 268, p. 1954–1959, doi:10.1016/j.nimb.2010.02.107.
- Babault, J., Bonnet, S., Crave, A., and Van den Driessche, J., 2005a, Influence of piedmont sedimentation on erosion dynamics of an uplifting landscape: An experimental approach: *Geology*, v. 33, p. 301–304.
- Babault, J., Van den Driessche, J., Bonnet, S., Castelltort, S., and Crave, A., 2005b, Origin of the highly elevated Pyrenean peneplain: *Tectonics*, v. 24.
- Balco, G., and Rovey, C.W., 2008, An isochron method for cosmogenic-nuclide dating of buried soils and sediments: *American Journal of Science*, v. 308, p. 1083–1114, doi:10.2475/10.2008.02.
- Balco, G., and Shuster, D.L., 2009,  $^{26}\text{Al}$ – $^{10}\text{Be}$ – $^{21}\text{Ne}$  burial dating: *Earth and Planetary Science Letters*, v. 286, p. 570–575, doi:10.1016/j.epsl.2009.07.025.
- Barrón, E., Rivas-Carballo, R., Postigo-Mijarra, J.M., Alcalde-Olivares, C., Vieira, M., Castro, L., Pais, J., and Valle-Hernández, M., 2010, The Cenozoic vegetation of the Iberian Peninsula: A synthesis: Review of Palaeobotany and Palynology, v. 162, p. 382–402, doi:10.1016/j.revpalbo.2009.11.007.
- Baynes, E.R.C., Lague, D., Steer, P., Bonnet, S., and Illien, L., 2020, Sediment flux-driven channel geometry adjustment of bedrock and mixed gravel–bedrock rivers: *Earth Surface Processes and Landforms*, v. 45, p. 3714–3731, doi:10.1002/esp.4996.



- Beamud, E., Garcés, M., Cabrera, L., Anton Muñoz, J., and Almar, Y., 2003, A new middle to late Eocene continental chronostratigraphy from NE Spain: *Earth and Planetary Science Letters*, v. 216, p. 501–514, doi:10.1016/S0012-821X(03)00539-9.
- Beamud, E., Muñoz, J.A., Fitzgerald, P.G., Baldwin, S.L., Garcés, M., Cabrera, L., and Metcalf, J.R., 2011, Magnetostratigraphy and detrital apatite fission track thermochronology in syntectonic conglomerates: constraints on the exhumation of the South-Central Pyrenees: *South-Central Pyrenees magnetostratigraphy and thermochronology: Basin Research*, v. 23, p. 309–331, doi:10.1111/j.1365-2117.2010.00492.x.
- Beaumont, C., Muñoz, J.A., Hamilton, J., and Fullsack, P., 2000, Factors controlling the Alpine evolution of the central Pyrenees inferred from a comparison of observations and geodynamical models: *Journal of Geophysical Research: Solid Earth*, v. 105, p. 8121–8145, doi:10.1029/1999JB900390.
- Benito, G., Gutiérrez, F., Pérez-González, A., and Machado, M.J., 2000, Geomorphological and sedimentological features in Quaternary fluvial systems affected by solution-induced subsidence (Ebro Basin, NE-Spain): *Geomorphology*, v. 33, p. 209–224.
- Benito, G., Pérez-González, A., Gutiérrez, F., and Machado, M.J., 1998, River response to Quaternary subsidence due to evaporite solution (Gállego River, Ebro Basin, Spain): *Geomorphology*, v. 22, p. 243–263, doi:10.1016/S0169-555X(97)00088-3.
- Benito, G., Sancho, C., Peña, J.L., Machado, M.J., and Rhodes, E.J., 2010, Large-scale karst subsidence and accelerated fluvial aggradation during MIS6 in NE Spain: climatic and paleohydrological implications: *Quaternary Science Reviews*, v. 29, p. 2694–2704, doi:10.1016/j.quascirev.2010.06.020.
- Bessais, E., and Cravatte, J., 1988, Les écosystèmes végétaux Pliocènes de Catalogne méridionale. Variations latitudinales dans le domaine nord-ouest méditerranéen: *Geobios*, v. 21, p. 49–63, doi:10.1016/S0016-6995(88)80031-7.
- Bierman, P.R., Gillespie, A.R., and Caffee, M.W., 1995, Cosmogenic Ages for Earthquake Recurrence Intervals and Debris Flow Fan Deposition, Owens Valley, California: *Science*, v. 270, p. 447–450.
- Bomer, B., 1979, Les Piedmonts du Bassin de l'Ebre (Espagne): *Méditerranée*, v. 36, p. 19–25, doi:10.3406/medit.1979.2178.
- Bosch, G.V., Teixell, A., Jolivet, M., Labaume, P., Stockli, D., Domènech, M., and Monié, P., 2016, Timing of Eocene–Miocene thrust activity in the Western Axial Zone and Chaînons Béarnais (west-central Pyrenees) revealed by multi-method thermochronology: *Comptes Rendus Geoscience*, v. 348, p. 246–256, doi:10.1016/j.crte.2016.01.001.
- Boschi, L., Faccenna, C., and Becker, T.W., 2010, Mantle structure and dynamic topography in the Mediterranean Basin: *MEDITERRANEAN MANTLE AND TOPOGRAPHY: Geophysical Research Letters*, v. 37, p. n/a–n/a, doi:10.1029/2010GL045001.
- Braucher, R., Guillou, V., Boulès, D.L., Arnold, M., Aumaître, G., Keddadouche, K., and Nottoli, E., 2015, Preparation of ASTER in-house  $^{10}\text{Be}/^{9}\text{Be}$  standard solutions: *Nuclear Instruments and Methods in Physics Research Section B: Beam Interactions with Materials and Atoms*, v. 361, p. 335–340, doi:10.1016/j.nimb.2015.06.012.

- Bridgland, D., and Westaway, R., 2008, Climatically controlled river terrace staircases: A worldwide Quaternary phenomenon: *Geomorphology*, v. 98, p. 285–315, doi:10.1016/j.geomorph.2006.12.032.
- Brown, E.T., Bourles, D.L., Raisbeck, G.M., Yiou, F., Clark Burchfiel, B., Molnar, P., Qidong, D., and Jun, L., 1998, Estimation of slip rates in the southern Tien Shan using cosmic ray exposure dates of abandoned alluvial fans: *Geological Society of America Bulletin*, v. 110, p. 377–386.
- Bufe, A., Burbank, D.W., Liu, L., Bookhagen, B., Qin, J., Chen, J., Li, T., Thompson Jobe, J.A., and Yang, H., 2017, Variations of Lateral Bedrock Erosion Rates Control Planation of Uplifting Folds in the Foreland of the Tian Shan, NW China: *Journal of Geophysical Research: Earth Surface*, v. 122, p. 2431–2467, doi:10.1002/2016JF004099.
- Bufe, A., Paola, C., and Burbank, D.W., 2016, Fluvial bevelling of topography controlled by lateral channel mobility and uplift rate: *Nature Geoscience*, v. 9, p. 706–710, doi:10.1038/ngeo2773.
- Calle, M., Sancho, C., Peña, J.L., Proença Cunha, P., Oliva-Urcia, B., and Pueyo, E.L., 2013, La secuencia de terrazas cuaternarias del río Alcanadre (provincia de Huesca): caracterización y consideraciones medioambientales: *Cuadernos de Investigación Geográfica*, v. 39, p. 159–178, doi:10.18172/cig.2004.
- Calvet, M., Gunnell, Y., Braucher, R., Hez, G., Bourlès, D., Guillou, V., and Delmas, M., 2015, Cave levels as proxies for measuring post-orogenic uplift: Evidence from cosmogenic dating of alluvium-filled caves in the French Pyrenees: *Geomorphology*, v. 246, p. 617–633, doi:10.1016/j.geomorph.2015.07.013.
- Calvet, M., Gunnell, Y., and Laumonier, B., 2020, Denudation history and palaeogeography of the Pyrenees and their peripheral basins: an 84-million-year geomorphological perspective: *Earth-Science Reviews*, p. 103436, doi:10.1016/j.earscirev.2020.103436.
- Carola, E., Muñoz, J.A., and Roca, E., 2015, The transition from thick-skinned to thin-skinned tectonics in the Basque-Cantabrian Pyrenees: the Burgalesa Platform and surroundings: *International Journal of Earth Sciences*, v. 104, p. 2215–2239, doi:10.1007/s00531-015-1177-z.
- Casas, A.M., Gil, I., Lerános, B., Millán, H., and Simón, L., 1994, Quaternary reactivation of flexural-slip folds by diapiric activity: example from the western Ebro Basin (Spain): *Geologische Rundschau*, v. 83, p. 853–867, doi:10.1007/BF00251081.
- Choukroune, P., 1989, Etude Continentale et Océanique par Reflexion et Refraction Sismique (ECORS) Team, The ECORS Pyrenean deep seismic profiles reflection data and the overall structure of an orogenic belt: *Tectonics*, v. 8, p. 23–39.
- Chumakov, I.S., 1967, Pliocene and Pleistocene deposits of the Nile valley in Nubian and Upper Egypt (in Russian): *Geol Institute Trans, Acad Science USSR, Moscow*, v. 170, p. 5.
- Cloetingh, S., Burov, E., Beekman, F., Andeweg, B., Andriessen, P. a. M., Garcia-Castellanos, D., Vicente, G. de, and Vegas, R., 2002, Lithospheric folding in Iberia: *Tectonics*, v. 21, p. 5-1-5–26, doi:https://doi.org/10.1029/2001TC901031.
- Coney, P.J., Muñoz, J.A., McClay, K.R., and Evenchick, C.A., 1996, Syntectonic burial and post-tectonic exhumation of the southern Pyrenees foreland fold-thrust belt: *Journal of the Geological Society*, v. 153, p. 9–16, doi:10.1144/gsjgs.153.1.0009.
- Conway-Jones, B.W., Roberts, G.G., Fichtner, A., and Hoggard, M., 2019, Neogene Epeirogeny of Iberia: *Geochemistry, Geophysics, Geosystems*, v. 20, p. 1138–1163, doi:10.1029/2018GC007899.

- Cook, K.L., Turowski, J.M., and Hovius, N., 2014, River gorge eradication by downstream sweep erosion: *Nature Geoscience*, v. 7, p. 682–686, doi:10.1038/ngeo2224.
- Cordier, S., Adamson, K., Delmas, M., Calvet, M., and Harmand, D., 2017, Of ice and water: Quaternary fluvial response to glacial forcing: *Quaternary Science Reviews*, v. 166, p. 57–73, doi:10.1016/j.quascirev.2017.02.006.
- Costa, E., Garcés, M., López-Blanco, M., Beamud, E., Gómez-Paccard, M., and Larrasoaña, J.C., 2010, Closing and continentalization of the South Pyrenean foreland basin (NE Spain): magnetochronological constraints: *Basin Research*, v. 22, p. 904–917, doi:10.1111/j.1365-2117.2009.00452.x.
- Craddock, W.H., Kirby, E., Harkins, N.W., Zhang, H., Shi, X., and Liu, J., 2010, Rapid fluvial incision along the Yellow River during headward basin integration: *Nature Geoscience*, v. 3, p. 209–213, doi:10.1038/ngeo777.
- Crosby, B.T., and Whipple, K.X., 2006, Knickpoint initiation and distribution within fluvial networks: 236 waterfalls in the Waipaoa River, North Island, New Zealand: *Geomorphology*, v. 82, p. 16–38, doi:10.1016/j.geomorph.2005.08.023.
- Del Rio, P., Barbero, L., and Stuart, F., 2009, Exhumation of the Sierra de Cameros (Iberian Range, Spain): constraints from low-temperature thermochronology: *Geological Society, London, Special Publications*, v. 324, p. 153–166.
- Delmas, M., 2019, L’apport des nucléides cosmogéniques produits in situ à la quantification multi-échelle des changements environnementaux quaternaires dans les montagnes des latitudes tempérées [HDR]: Université Lumière Lyon 2.
- Delmas, M., Calvet, M., Gunnell, Y., Voinchet, P., Manel, C., Braucher, R., Tissoux, H., Bahain, J.-J., Perrenoud, C., and Saos, T., 2018, Terrestrial  $^{10}\text{Be}$  and electron spin resonance dating of fluvial terraces quantifies quaternary tectonic uplift gradients in the eastern Pyrenees: *Quaternary Science Reviews*, v. 193, p. 188–211, doi:10.1016/j.quascirev.2018.06.001.
- Dunai, T.J., 2010, *Cosmogenic nuclides: principles, concepts and applications in the earth surface sciences*: Cambridge; New York, Cambridge University Press, <http://dx.doi.org/10.1017/CBO9780511804519> (accessed August 2017).
- Duval, M., Arnold, L.J., Guilarte, V., Demuro, M., Santonja, M., and Pérez-González, A., 2017, Electron spin resonance dating of optically bleached quartz grains from the Middle Palaeolithic site of Cuesta de la Bajada (Spain) using the multiple centres approach: *Quaternary Geochronology*, v. 37, p. 82–96, doi:10.1016/j.quageo.2016.09.006.
- Duval, M., Sancho, C., Calle, M., Guilarte, V., and Peña-Monné, J.L., 2015, On the interest of using the multiple center approach in ESR dating of optically bleached quartz grains: Some examples from the Early Pleistocene terraces of the Alcanadre River (Ebro basin, Spain): *Quaternary Geochronology*, v. 29, p. 58–69, doi:10.1016/j.quageo.2015.06.006.
- Etheve, N., Mohn, G., Lamotte, D.F. de, Roca, E., Tugend, J., and Gómez-Romeu, J., 2018, Extreme Mesozoic Crustal Thinning in the Eastern Iberia Margin: The Example of the Columbrets Basin (Valencia Trough): *Tectonics*, v. 37, p. 636–662, doi:10.1002/2017TC004613.
- Evans, G., and Arche, A., 2002, The flux of siliciclastic sediment from the Iberian Peninsula, with particular reference to the Ebro: *Geological Society, London, Special Publications*, v. 191, p. 199–208.

- Faccenna, C. et al., 2014, Mantle dynamics in the Mediterranean: Mediterranean Dynamic: Reviews of Geophysics, v. 52, p. 283–332, doi:10.1002/2013RG000444.
- Fillon, C. et al., 2020, Post-orogenic exhumation in the western Pyrenees: evidence for extension driven by pre-orogenic inheritance: Journal of the Geological Society, doi:10.1144/jgs2020-079.
- Fillon, C., Gautheron, C., and van der Beek, P., 2013, Oligocene–Miocene burial and exhumation of the Southern Pyrenean foreland quantified by low-temperature thermochronology: Journal of the Geological Society, v. 170, p. 67–77.
- Fillon, C., Pedreira, D., van der Beek, P.A., Huismans, R.S., Barbero, L., and Pulgar, J.A., 2016, Alpine exhumation of the central Cantabrian Mountains, Northwest Spain: Alpine exhumation of the Cantabrians: Tectonics, v. 35, p. 339–356, doi:10.1002/2015TC004050.
- Fitzgerald, P.G., Muñoz, J.A., Coney, P.J., and Baldwin, S.L., 1999, Asymmetric exhumation across the Pyrenean orogen: implications for the tectonic evolution of a collisional orogen: Earth and Planetary Science Letters, v. 173, p. 157–170, doi:10.1016/S0012-821X(99)00225-3.
- Fontboté, J., Guimerà, J., Roca, E., Sàbat, F., Santanach, P., and Fernández-Ortigosa, F., 1990, The Cenozoic geodynamic evolution of the Valencia trough (western Mediterranean): Rev. Soc. Geol. Esp., v. 3, p. 249–259.
- Fornari, M., Risacher, F., and Féraud, G., 2001, Dating of paleolakes in the central Altiplano of Bolivia: Palaeogeography, Palaeoclimatology, Palaeoecology, v. 172, p. 269–282, doi:10.1016/S0031-0182(01)00301-7.
- Fuller, I.C., Macklin, M.G., Lewin, J., Passmore, D.G., and Wintle, A.G., 1998, River response to high-frequency climate oscillations in southern Europe over the past 200 k.y.: Geology, v. 26, p. 275–278, doi:10.1130/0091-7613(1998)026<0275:RRTHFC>2.3.CO;2.
- Fuller, I.C., Macklin, M.G., Passmore, D.G., Brewer, P.A., Lewin, J., and Wintle, A.G., 1996, Geochronologies and environmental records of Quaternary fluvial sequences in the Guadalope basin, northeast Spain, based on luminescence dating: Geological Society, London, Special Publications, v. 115, p. 99–120, doi:10.1144/GSL.SP.1996.115.01.09.
- García-Castellanos, D., 2006, Long-term evolution of tectonic lakes: climatic controls on the development of internally drained basins: Special Papers-Geological Society of America, v. 398, p. 283.
- García-Castellanos, D., and Larrasoña, J.C., 2015, Quantifying the post-tectonic topographic evolution of closed basins: The Ebro basin (northeast Iberia): Geology, v. 43, p. 663–666, doi:10.1130/G36673.1.
- García-Castellanos, D., Vergés, J., Gaspar-Escribano, J., and Cloetingh, S., 2003, Interplay between tectonics, climate, and fluvial transport during the Cenozoic evolution of the Ebro Basin (NE Iberia): Tectonics, Climate, and Drainage: Journal of Geophysical Research: Solid Earth, v. 108, doi:10.1029/2002JB002073.
- García-Ruiz, J.M., Martí-Bono, C., Peña-Monné, J.L., Sancho, C., Rhodes, E.J., Valero-garcés, B., González-sampériz, P., and Moreno, A., 2013, Glacial and fluvial deposits in the aragón valley, central-western pyrenees: chronology of the pyrenean late pleistocene glaciers: Geografiska Annaler: Series A, Physical Geography, v. 95, p. 15–32, doi:10.1111/j.1468-0459.2012.00478.x.

- Gaspar-Escribano, J.M., Garcia-Castellanos, D., Roca, E., and Cloetingh, S., 2004, Cenozoic vertical motions of the Catalan Coastal Ranges (NE Spain): The role of tectonics, isostasy, and surface transport: *Tectonics*, v. 23, doi:10.1029/2003TC001511.
- Genti, M., 2015, Impact des processus de surface sur la déformation actuelle des Pyrénées et des Alpes [PhD Thesis]: Université de Montpellier, 263 p.
- Gibbard, P.L., and Lewin, J., 2009, River incision and terrace formation in the Late Cenozoic of Europe: *Tectonophysics*, v. 474, p. 41–55, doi:10.1016/j.tecto.2008.11.017.
- Gibson, M., Sinclair, H.D., Lynn, G.J., and Stuart, F.M., 2007, Late- to post-orogenic exhumation of the Central Pyrenees revealed through combined thermochronological data and modelling: *Basin Research*, v. 19, p. 323–334, doi:10.1111/j.1365-2117.2007.00333.x.
- Gosse, J.C., and Phillips, F.M., 2001, Terrestrial in situ cosmogenic nuclides: theory and application: *Quaternary Science Reviews*, v. 20, p. 1475–1560.
- Guerrero, J., Gutiérrez, F., and Galve, J.P., 2013, Large depressions, thickened terraces, and gravitational deformation in the Ebro River valley (Zaragoza area, NE Spain): Evidence of glauberite and halite interstratal karstification: *Geomorphology*, v. 196, p. 162–176, doi:10.1016/j.geomorph.2012.06.024.
- Guerrero, J., Gutiérrez, F., and Lucha, P., 2008, Impact of halite dissolution subsidence on Quaternary fluvial terrace development: Case study of the Huerva River, Ebro Basin, NE Spain: *Geomorphology*, v. 100, p. 164–179, doi:10.1016/j.geomorph.2007.04.040.
- Han, Z. et al., 2019, Internal Drainage Has Sustained Low-Relief Tibetan Landscapes Since the Early Miocene: *Geophysical Research Letters*, v. 46, p. 8741–8752, doi:https://doi.org/10.1029/2019GL083019.
- Haug, G.H., and Tiedemann, R., 1998, Effect of the formation of the Isthmus of Panama on Atlantic Ocean thermohaline circulation: *Nature*, v. 393, p. 673–676.
- Hidy, A.J., Gosse, J.C., Pederson, J.L., Mattern, J.P., and Finkel, R.C., 2010, A geologically constrained Monte Carlo approach to modeling exposure ages from profiles of cosmogenic nuclides: An example from Lees Ferry, Arizona: *Geochemistry Geophysics Geosystems*, v. 11, doi:10.1029/2010GC003084.
- Huyghe, D., Mouthereau, F., Ségalen, L., and Furió, M., 2020, Long-term dynamic topographic support during post-orogenic crustal thinning revealed by stable isotope ( $\delta^{18}\text{O}$ ) paleo-altimetry in eastern Pyrenees: *Scientific Reports*, v. 10, doi:10.1038/s41598-020-58903-w.
- Jiménez-Moreno, G., Burjachs, F., Expósito, I., Oms, O., Carrancho, Á., Villalaín, J.J., Agustí, J., Campeny, G., de Soler, B.G., and van der Made, J., 2013, Late Pliocene vegetation and orbital-scale climate changes from the western Mediterranean area: *Global and Planetary change*, v. 108, p. 15–28.
- Jolivet, M., Labaume, P., Monié, P., Brunel, M., Arnaud, N., and Campani, M., 2007, Thermochronology constraints for the propagation sequence of the south Pyrenean basement thrust system (France-Spain): *Tectonics*, v. 26.
- Julián Andrés, A., 1996, Cartografía y correlación general de las acumulaciones cuaternarias de la depresión del Ebro [PhD Thesis]: Universidad de Zaragoza.
- Julián Andrés, A., and Chueca Cía, J.J., 1998, Acumulaciones fluviales en la Depresión del Ebro: valoración de la validez de una secuencia general: *Geographica*, p. 67–82.



- Jungers, M.C., and Heimsath, A.M., 2016, Post-tectonic landscape evolution of a coupled basin and range: Pinaleno Mountains and Safford Basin, southeastern Arizona: *Geological Society of America Bulletin*, v. 128, p. 469–486, doi:10.1130/B31276.1.
- Knudsen, M.F., Nørgaard, J., Grischott, R., Kober, F., Egholm, D.L., Hansen, T.M., and Jansen, J.D., 2020, New cosmogenic nuclide burial-dating model indicates onset of major glaciations in the Alps during Middle Pleistocene Transition: *Earth and Planetary Science Letters*, v. 549, p. 116491, doi:10.1016/j.epsl.2020.116491.
- Labaume, P., Meresse, F., Jolivet, M., Teixell, A., and Lahfid, A., 2016, Tectonothermal history of an exhumed thrust-sheet-top basin: An example from the south Pyrenean thrust belt: *Tectonics*, v. 35, p. 1280–1313, doi:10.1002/2016TC004192.
- Lal, D., 1991, Cosmic ray labeling of erosion surfaces: in-situ nuclide production rates and erosion models: *Earth Planet. Sci. Lett.*, v. 104, p. 424–439.
- Larrasoana, J.C., Murelaga, X., and Garcés, M., 2006, Magnetobiochronology of Lower Miocene (Ramblian) continental sediments from the Tudela Formation (western Ebro basin, Spain): *Earth and Planetary Science Letters*, v. 243, p. 409–423, doi:10.1016/j.epsl.2006.01.034.
- Lewis, C.J., McDonald, E.V., Sancho, C., Peña, J.L., and Rhodes, E.J., 2009, Climatic implications of correlated Upper Pleistocene glacial and fluvial deposits on the Cinca and Gállego Rivers (NE Spain) based on OSL dating and soil stratigraphy: *Global and Planetary Change*, v. 67, p. 141–152, doi:10.1016/j.gloplacha.2009.01.001.
- Lewis, C.J., Sancho, C., McDonald, E.V., Peña-Monné, J.L., Pueyo, E.L., Rhodes, E., Calle, M., and Soto, R., 2017, Post-tectonic landscape evolution in NE Iberia using staircase terraces: Combined effects of uplift and climate: *Geomorphology*, v. 292, p. 85–103, doi:10.1016/j.geomorph.2017.04.037.
- Lewis, C.J., Vergés, J., and Marzo, M., 2000, High mountains in a zone of extended crust: Insights into the Neogene-Quaternary topographic development of northeastern Iberia: *Tectonics*, v. 19, p. 86–102, doi:https://doi.org/10.1029/1999TC900056.
- Lisiecki, L.E., and Raymo, M.E., 2005, A Pliocene-Pleistocene stack of 57 globally distributed benthic delta O-18 records (vol 20, art no PA1003, 2005): *Paleoceanography*, v. 20, p. PA2007, doi:10.1029/2005PA001164.
- Loget, N., Driessche, J.V.D., and Davy, P., 2005, How did the Messinian salinity crisis end? *Terra Nova*, v. 17, p. 414–419.
- Loget, N., and Van Den Driessche, J., 2009, Wave train model for knickpoint migration: *Geomorphology*, v. 106, p. 376–382.
- López Martínez, N., Agustí, J., Cabrera, L., Calvo Sorando, J., Civis, J., Corrochano, A., Daams, R., Díaz Esteban, M., Elizaga, E., and Hoyos Gómez, M., 1987, Approach to the Spanish continental Neogene synthesis and palaeoclimatic interpretation.: *Ann. Inst. Geol. Publ. Hung.*, v. LXX, p. 383–391.
- López-Blanco, M., 2002, Sedimentary response to thrusting and fold growing on the SE margin of the Ebro basin (Paleogene, NE Spain): *Sedimentary Geology*, v. 146, p. 133–154.
- Lucha, P., Gutiérrez, F., Galve, J.P., and Guerrero, J., 2012, Geomorphic and stratigraphic evidence of incision-induced halokinetic uplift and dissolution subsidence in transverse drainages crossing the evaporite-cored Barbastro–Balaguer Anticline (Ebro Basin, NE Spain): *Geomorphology*, v. 171–172, p. 154–172, doi:10.1016/j.geomorph.2012.05.015.

- Macklin, M.G., Fuller, I.C., Lewin, J., Maas, G.S., Passmore, D.G., Rose, J., Woodward, J.C., Back, S., Hamlin, R.H.B., and Rowan, J.S., 2002, Correlation of fluvial sequences in the Mediterranean basin over the last 200 ka and their relationship to climate change: *Quaternary Sci. Rev.*, v. 21, p. 1633–1641.
- Maier-Reimer, E., Mikolajewicz, U., and Crowley, T., 1990, Ocean general circulation model sensitivity experiment with an open Central American Isthmus: *Paleoceanography*, v. 5, p. 349–366.
- Mensua, S., and Ibañez, M.J., 1977, Terrazas y glaciares del centro de la depresión del Ebro (5 mapas y Comentario): Departamento de Geografía.
- Mocochain, L., Audra, P., Clauzon, G., Bellier, O., Bigot, J.-Y., Parize, O., and Monteil, P., 2009, The effect of river dynamics induced by the Messinian Salinity Crisis on karst landscape and caves: example of the Lower Ardèche river (mid Rhône valley): *Geomorphology*, v. 106, p. 46–61.
- Molnar, P., 2008, Closing of the Central American Seaway and the Ice Age: A critical review: *Paleoceanography*, v. 23.
- Monod, B., Regard, V., Carcone, J., Wyns, R., and Christophoul, F., 2016, Postorogenic planar palaeosurfaces of the central Pyrenees: Weathering and neotectonic records: *Comptes Rendus Geoscience*, v. 348, p. 184–193, doi:10.1016/j.crte.2015.09.005.
- Moreno, D. et al., 2012, ESR chronology of alluvial deposits in the Arlanzón valley (Atapuerca, Spain): Contemporaneity with Atapuerca Gran Dolina site: *Quaternary Geochronology*, v. 10, p. 418–423, doi:10.1016/j.quageo.2012.04.018.
- Morris, Sinclair, and Yell, 1998, Exhumation of the Pyrenean orogen: implications for sediment discharge: *Basin Research*, v. 10, p. 69–85, doi:10.1046/j.1365-2117.1998.00053.x.
- Mouthereau, F., Filleaudeau, P.-Y., Vacherat, A., Pik, R., Lacombe, O., Fellin, M.G., Castelltort, S., Christophoul, F., and Masini, E., 2014, Placing limits to shortening evolution in the Pyrenees: Role of margin architecture and implications for the Iberia/Europe convergence: Plate convergence in the Pyrenees: *Tectonics*, v. 33, p. 2283–2314, doi:10.1002/2014TC003663.
- Muñoz, J.A., 1992, Evolution of a continental collision belt: ECORS-Pyrenees crustal balanced cross-section, *in* Thrust tectonics, Springer, p. 235–246.
- Muñoz, J., Martínez, A., and Vergés, J., 1986, Thrust sequences in the eastern Spanish Pyrenees: *Journal of Structural Geology*, v. 8, p. 399–405.
- Peña-Monné, J., and Sancho, C., 1988, Correlación y evolución cuaternaria del sistema fluvial Segre-Cinca en su curso bajo (provs. de Lérida y Huesca): *Cuaternario y geomorfología*, v. 2, p. 77–83.
- Pérez-Rivarés, J., Crespo, M.G., Abad, M.C.A., and Tirapu, G.P., 2004, Magnetostratigraphy of the Miocene continental deposits of the Montes de Castejón (central Ebro basin, Spain): geochronological and paleoenvironmental implications: *Geologica Acta*, v. 2, p. 221–234.
- Pérez-Rivarés, F., Garcés, M., Arenas, C., and Pardo, G., 2002, Magnetocronología de la sucesión miocena de la Sierra de Alcubierre (sector central de la Cuenca del Ebro): *Revista de la Sociedad Geológica de España*, v. 15, p. 217–231.
- Puigdefàbregas, C., Muñoz, J.A., and Vergés, J., 1992, Thrusting and foreland basin evolution in the Southern Pyrenees, *in* McClay, K.R. ed., Thrust Tectonics, Dordrecht, Springer Netherlands, p. 247–254, doi:10.1007/978-94-011-3066-0\_22.

- Rat, J., Mouthereau, F., Brichau, S., Crémades, A., Bernet, M., Balvay, M., Ganne, J., Lahfid, A., and Gautheron, C., 2019, Tectonothermal Evolution of the Cameros Basin: Implications for Tectonics of North Iberia: *Tectonics*, v. 38, p. 440–469, doi:10.1029/2018TC005294.
- Regard, V. et al., 2005, Cumulative right-lateral fault slip rate across the Zagros-Makran transfer zone: role of the Minab-Zendan fault system in accommodating Arabia-Eurasia convergence in southeast Iran: *Geophysical Journal International*, v. 162, p. 177–203.
- Repka, J.L., Anderson, R.S., and Finkel, R.C., 1997, Cosmogenic dating of fluvial terraces, Fremont River, Utah: *Earth And Planetary Science Letters*, v. 152, p. 59–73.
- Ritz, J.F. et al., 2003, Late Pleistocene to Holocene slip rates for the Gurvan Bulag thrust fault (Gobi-Altay, Mongolia) estimated with Be-10 dates: *Journal Of Geophysical Research-Solid Earth*, v. 108.
- Roca, E., Desegaulx, P., Fernandez Ortigosa, F., Roure, F., and Pinet, B., 1990, *in* Pinet, B. and Bois, C. eds., *The Potential of Deep Seismic Profiling for Hydrocarbon Exploration: Proceedings of the 5th IFP Exploration and Production Research Conference, Held in Arles, June 19-23, 1989*, Paris, p. 439–443.
- Roca, E., and Guimerà, J., 1992, The Neogene structure of the eastern Iberian margin: Structural constraints on the crustal evolution of the Valencia trough (western Mediterranean): *Tectonophysics*, v. 203, p. 203–218, doi:10.1016/0040-1951(92)90224-T.
- Roca, E., Sans, M., Cabrera, L., and Marzo, M., 1999, Oligocene to Middle Miocene evolution of the central Catalan margin (northwestern Mediterranean): *Tectonophysics*, v. 315, p. 209–229, doi:10.1016/S0040-1951(99)00289-9.
- Rodríguez-Rodríguez, L. et al., 2020, Dates and rates of endo-exorheic drainage development: Insights from fluvial terraces (Duero River, Iberian Peninsula): *Global and Planetary Change*, v. 193, p. 103271, doi:10.1016/j.gloplacha.2020.103271.
- Roure, F., Choukroune, P., Berastegui, X., Munoz, J., Villien, A., Matheron, P., Bareyt, M., Seguret, M., Camara, P., and Deramond, J., 1989, ECORS deep seismic data and balanced cross sections: Geometric constraints on the evolution of the Pyrenees: *Tectonics*, v. 8, p. 41–50.
- Rushlow, C.R., Barnes, J.B., Ehlers, T.A., and Vergés, J., 2013, Exhumation of the southern Pyrenean fold-thrust belt (Spain) from orogenic growth to decay: *Tectonics*, v. 32, p. 843–860, doi:10.1002/tect.20030.
- Sàbat, F., Roca, E., Muñoz, J., Vergés, J., Santanach, P., and Sans, M., 1995, margin of Iberia: the ESCI-València Trough seismic profile: *Rev. Soc. Geol. España*, v. 8, p. 4.
- Salas, R., and Casas, A., 1993, Mesozoic extensional tectonics, stratigraphy and crustal evolution during the Alpine cycle of the eastern Iberian basin: *Tectonophysics*, v. 228, p. 33–55, doi:10.1016/0040-1951(93)90213-4.
- Salas, R., Guimerà, J., Mas, R., Martín-Closas, C., Meléndez, A., and Alonso, A., 2001, Evolution of the Mesozoic central Iberian Rift System and its Cainozoic inversion (Iberian chain): *Peri-Tethys Memoir*, v. 6, p. 145–185.
- Sancho, C., Arenas, C., Pardo, G., Peña-Monné, J.L., Rhodes, E.J., Bartolomé, M., García-Ruiz, J.M., and Martí-Bono, C., 2018, Glaciolacustrine deposits formed in an ice-dammed tributary valley in the south-central Pyrenees: New evidence for late Pleistocene climate: *Sedimentary Geology*, v. 366, p. 47–66, doi:10.1016/j.sedgeo.2018.01.008.

- Sancho, C., Calle, M., Pena-Monne, J.L., Duval, M., Oliva-Urcia, B., Pueyo, E.L., Benito, G., and Moreno, A., 2016, Dating the Earliest Pleistocene alluvial terrace of the Alcanadre River (Ebro Basin, NE Spain): Insights into the landscape evolution and involved processes: *Quaternary International*, v. 407, p. 86–95, doi:10.1016/j.quaint.2015.10.050.
- Santisteban, J.I., and Schulte, L., 2007, Fluvial networks of the Iberian Peninsula: a chronological framework: *Quaternary Science Reviews*, v. 26, p. 2738–2757, doi:10.1016/j.quascirev.2006.12.019.
- Saura, E., Ardèvol i Oró, L., Teixell, A., and Vergés, J., 2016, Rising and falling diapirs, shifting depocenters, and flap overturning in the Cretaceous Sopeira and Sant Gervàs subbasins (Ribagorça Basin, southern Pyrenees): *Tectonics*, v. 35, p. 638–662, doi:10.1002/2015TC004001.
- Siddall, M., Honisch, B., Waelbroeck, C., and Huybers, P., 2010, Changes in deep Pacific temperature during the mid-Pleistocene transition and Quaternary: *Quaternary Science Reviews*, v. 29, p. 170–181.
- Sinclair, H.D., Gibson, M., Naylor, M., and Morris, R.G., 2005, Asymmetric growth of the Pyrenees revealed through measurement and modeling of orogenic fluxes: *American Journal of Science*, v. 305, p. 369–406, doi:10.2475/ajs.305.5.369.
- Sobel, E.R., Hilley, G.E., and Strecker, M.R., 2003, Formation of internally drained contractional basins by aridity-limited bedrock incision: *Journal of Geophysical Research: Solid Earth*, v. 108, doi:10.1029/2002JB001883.
- Soria Jáuregui, Á., González Amuchastegui, M.J., Serrano Cañadas, E., Edeso Fito, J.M., Lopetegi Galarraga, A., Duval, M., and Parés, J.M., 2019, Las terrazas fluviales cuaternarias del río Ebro en el alto Ebro (Incinillas-Conchas de Haro), in *Asociación Española para el Estudio del Cuaternario (AEQUA)*, <https://cir.cenieh.es/handle/20.500.12136/1418> (accessed February 2020).
- Stange, K.M., Balen, R.T.V., Garcia-Castellanos, D., and Cloetingh, S., 2016, Numerical modelling of Quaternary terrace staircase formation in the Ebro foreland basin, southern Pyrenees, NE Iberia: *Basin Research*, v. 28, p. 124–146, doi:10.1111/bre.12103.
- Stange, K.M., van Balen, R., Carcaillet, J., and Vandenberghe, J., 2013a, Terrace staircase development in the Southern Pyrenees Foreland: Inferences from  $^{10}\text{Be}$  terrace exposure ages at the Segre River: *Global and Planetary Change*, v. 101, p. 97–112, doi:10.1016/j.gloplacha.2012.12.007.
- Stange, K.M., van Balen, R., Vandenberghe, J., Peña, J.L., and Sancho, C., 2013b, External controls on Quaternary fluvial incision and terrace formation at the Segre River, Southern Pyrenees: *Tectonophysics*, v. 602, p. 316–331, doi:10.1016/j.tecto.2012.10.033.
- Struth, L., Garcia-Castellanos, D., Viaplana-Muzas, M., and Vergés, J., 2019, Drainage network dynamics and knickpoint evolution in the Ebro and Duero basins: From endorheism to exorheism: *Geomorphology*, v. 327, p. 554–571, doi:10.1016/j.geomorph.2018.11.033.
- Suc, J.-P., and Popescu, S.-M., 2005, Pollen records and climatic cycles in the North Mediterranean region since 2.7 Ma: *Geological Society, London, Special Publications*, v. 247, p. 147–158.
- Teixell, A., 1990, Alpine thrusts at the western termination of the Pyrenean axial zone: *Bulletin de la Société Géologique de France*, v. VI, p. 241–249, doi:10.2113/gssgfbull.VI.2.241.
- Teixell, A., 1998, Crustal structure and orogenic material budget in the west central Pyrenees: *Tectonics*, v. 17, p. 395–406, doi:10.1029/98TC00561.

- Teixell, A., 1996, The Ansó transect of the southern Pyrenees: basement and cover thrust geometries: *Journal of the Geological Society*, v. 153, p. 301–310, doi:10.1144/gsjgs.153.2.0301.
- Tziperman, E., and Gildor, H., 2003, On the mid-Pleistocene transition to 100-kyr glacial cycles and the asymmetry between glaciation and deglaciation times: *Paleoceanography*, v. 18, p. 1–1.
- Urgeles, R., Camerlenghi, A., Garcia-Castellanos, D., De Mol, B., Garcés, M., Vergés, J., Haslam, I., and Hardman, M., 2011, New constraints on the Messinian sealevel drawdown from 3D seismic data of the Ebro Margin, western Mediterranean: *Basin Research*, v. 23, p. 123–145.
- Vacherat, A., Bonnet, S., and Mouthereau, F., 2018, Drainage reorganization and divide migration induced by the excavation of the Ebro basin (NE Spain): *Earth Surface Dynamics*, v. 6, p. 369–387, doi:<https://doi.org/10.5194/esurf-6-369-2018>.
- Vázquez-Urbez, M., Arenas, C., Pardo, G., and Pérez-Rivarés, J., 2013, The Effect of Drainage Reorganization and Climate On the Sedimentologic Evolution of Intermontane Lake Systems: The Final Fill Stage of the Tertiary Ebro Basin (Spain): *Journal of Sedimentary Research*, v. 83, p. 562–590, doi:10.2110/jsr.2013.47.
- Vergés, J., Fernández, M., and Martínez, A., 2002, The Pyrenean orogen: pre-, syn-, and post-collisional evolution: *Journal of the Virtual Explorer*, v. 8, p. 55–74.
- Vergés, J., Millán, H., Roca, E., Muñoz, J., Marzo, M., Cirés, J., Den Bezemer, T., Zoetemeijer, R., and Cloetingh, S., 1995, Eastern Pyrenees and related foreland basins: pre-, syn- and post-collisional crustal-scale cross-sections: *Marine and Petroleum geology*, v. 12, p. 903–915.
- Vincent, S.J., 2001, The Sis palaeovalley: a record of proximal fluvial sedimentation and drainage basin development in response to Pyrenean mountain building: *Sedimentology*, v. 48, p. 1235–1276, doi:10.1046/j.1365-3091.2001.00421.x.
- Whitchurch, A.L., Carter, A., Sinclair, H.D., Duller, R.A., Whittaker, A.C., and Allen, P.A., 2011, Sediment routing system evolution within a diachronously uplifting orogen: Insights from detrital zircon thermochronological analyses from the South-Central Pyrenees: *American Journal of Science*, v. 311, p. 442–482, doi:10.2475/05.2011.03.
- Yelland, A., 1990, Fission track thermotectonics in the Pyrenean orogen: *International Journal of Radiation Applications and Instrumentation. Part D. Nuclear Tracks and Radiation Measurements*, v. 17, p. 293–299.